TRIBHUVAN UNIVERSITY

INSTITUTE OF ENGINEERING

PULCHOWK CAMPUS

THESIS NO: PUL080MSMSE005

MOF-DERIVED CARBON COMPOSITES FROM JACARANDA SEED PODS FOR SELECTIVE REMOVAL OF HEXAVALENT CHROMIUM [CR(VI)]

by

BIBEK GHIMIRE

A THESIS

SUBMITTED TO THE DEPARTMENT OF APPLIED SCIENCES AND CHEMICAL ENGINEERING

IN PARTIAL FULFILLMENT OF THE REQUIREMENTS FOR THE

DEGREE OF MASTER OF SCIENCE IN MATERIAL SCIENCE AND ENGINEERING

DEPARTMENT OF APPLIED SCIENCES AND CHEMICAL ENGINEERING

LALITPUR, NEPAL

MAY 2026

COPYRIGHT

BOARD OF EXAMINATION AND CERTIFICATE OF APPROVAL

This thesis entitled "**MOF-Derived Carbon Composites from Jacaranda Seed Pods for Selective Removal of Hexavalent Chromium [Cr(VI)]**" by Mr. Bibek Ghimire (Campus Roll No. PUL080MSMSE005 and T.U. Registration 3-2-26-66-2015) under the supervision of Asst. Prof. Dr. Tanka Mukhiya, Department of Applied Sciences and Chemical Engineering, Pulchowk Campus, Institute of Engineering, Tribhuvan University, is hereby submitted for the partial fulfilment of the Master of Science (M.Sc.) degree in Material Science and Engineering. This report has been accepted and forwarded to the Controller of Examination, Institute of Engineering, Tribhuvan University, Nepal for the legal procedure.

Dr. Tanka Mukhiya
Supervisor
Assistant Professor
Department of Applied Sciences and Chemical Engineering
Pulchowk Campus, Institute of Engineering
Tribhuvan University, Nepal

Dr. Deval Prasad Bhattarai
External Examiner
Assistant Professor
Department of Chemistry
Amrit Campus
Tribhuvan University, Nepal

Prof. Dr. Sahira Joshi
Head of Department
Department of Applied Sciences and Chemical Engineering, Pulchowk Campus
Institute of Engineering
Tribhuvan University, Nepal

RECOMMENDATION

This is to recommend that Mr. Bibek Ghimire (Campus Roll No. PUL080MSMSE005 and T.U. Registration 3-2-26-66-2015) has carried out the thesis work entitled "**MOF-Derived Carbon Composites from Jacaranda Seed Pods for Selective Removal of Hexavalent Chromium [Cr(VI)]**" as part of the requirements for the Master of Science (M.Sc.) degree in Materials Science and Engineering under my supervision in the Department of Applied Sciences & Chemical Engineering, Pulchowk Campus, Institute of Engineering, Tribhuvan University, Kathmandu, Nepal.

He has fulfilled all the requirements laid down by the Institute of Engineering, Tribhuvan University, Nepal for the submission of the thesis work for the partial fulfillment of Master of Science (M.Sc.) degree in Material Science and Engineering.

……

Dr. Tanka Mukhiya

Supervisor

Assistant Professor

Department of Applied Sciences and Chemical Engineering

Pulchowk Campus

Tribhuvan University, Nepal

DECLARATION

This thesis entitled "**MOF-Derived Carbon Composites from Jacaranda Seed Pods for Selective Removal of Hexavalent Chromium [Cr(VI)]**" is submitted to the Department of Applied Sciences & Chemical Engineering, Pulchowk Campus, Institute of Engineering, Tribhuvan University, Nepal for the partial fulfillment of the requirements for the Master of Science (M.Sc.) degree in Material Science and Engineering. This thesis work is carried out by me under the supervision of Assistant Professor Dr. Tanka Mukhiya, Department of Applied Sciences and Chemical Engineering, Institute of Engineering, Pulchowk Campus, Tribhuvan University, Nepal.

This work was done by me originally and has not been submitted earlier, for the award of any other degree.

Bibek Ghimire
Roll No 080MSMSE005
T.U. Registration No. 3-2-26-66-2015

ACKNOWLEDGEMENTS

I am deeply grateful to my supervisor Dr. Tanka Mukhiya from the Department of Applied Sciences and Chemical Engineering, Pulchowk Campus, Tribhuvan University; for his insightful suggestions, invaluable guidance and motivation for conducting and completion of my thesis work. I am also grateful to Professor Dr. Sahira Joshi, Head of Department; and Dr. Ganesh Kumar Shrestha, Program Coordinator, Department of Applied Sciences and Chemical Engineering, for their assistance and for creating a favorable academic atmosphere in which to conduct this research.

I would like to thank Nanomaterials Laboratory for providing the required facilities to conduct the experiment. I am particularly grateful to Amrit Campus for supporting the FTIR study and Jeonbuk National University in South Korea for providing FESEM, EDX and XRD characterization. I would like to appreciate **Nepal Academy of Science and Technology (NAST)** for providing master's thesis grant 2082-2083.

I would like to express sincere appreciation to Dr. Milan Babu Poudel, Mr. Rajesh Shrestha and Mr. Aek Narayan Kamal for their invaluable support with the characterization and carbonization of the samples, which was critical to the success of this project. Furthermore, I'd also like to thank my friends, Mr. Ashman Karki, Ms. Bipana Ojha Khatri, Mr. Sachin Ghimire and Ms. Charu Gajurel for their constructive feedback and technical assistance throughout this journey.

Finally, I express my deepest gratitude to my family for their unwavering support, encouragement, and inspiration. Their patience and belief in me have been a constant source of strength, and I owe the successful completion of this thesis to them.

Bibek Ghimire

LIST OF ACRONYMS AND ABBREBIATION

°C	Degree Celsius
BET	Brunauer–Emmett–Teller
Cr(III)	Trivalent Chromium
Cr(VI)	Hexavalent Chromium
DI Water	Deionized Water
DPC	1,5-Diphenylcarbazide
EDX	Energy Dispersive X-ray Spectroscopy
FTIR	Fourier Transform Infrared Spectroscopy
JSP	Jacaranda Seed Pods
MOF	Metal-Organic Framework
PFO	Pseudo-First-Order
PSO	Pseudo-Second-Order
rpm	Revolutions Per Minute
SEM	Scanning Electron Microscopy
UV–Vis	Ultraviolet–Visible Spectroscopy
XRD	X-ray Diffraction
ZIF-67	Zeolitic Imidazolate Framework-67

LIST OF SYMBOLS

%	Percentage
µm	Micrometer
Co	Cobalt
g	Gram
h	Hours
K	Kelvin
L	Liter
m	Meter
mg	Milligram
mIm	Methylimidazole
mL	Milliliter
nm	Nanometer
ºC	Degree Celsius
µA	Microampere
ppm	Parts per million
λ	Wave length
rpm	Revolutions per minute

ABSTRACT

Heavy metal contamination is being as a global emerging issue in this 21st Century. Hexavalent chromium [Cr(VI)] constitutes one of the emerging pollutants that pose significant threat owing to their persistence, bioaccumulation potential and major impact on human health. The conventional techniques are not able to remove such heavy metal impurities effectively and its purification is somehow challenging in a minute level. In this study, a carbon composite was fabricated from Zeolitic Imidazolate Framework-67 (ZIF-67) via in-situ process on a jacaranda seed pods biomass substrate and carbonized it in an inert atmosphere by passing nitrogen gas in a tube furnace at three temperatures 700 ºC, 800 ºC and 900 ºC. The resultant MOF-derived carbon composite was characterized with respect to FTIR, FESEM, EDX and XRD analysis. Furthermore, the adsorption capacity of the synthesized material was studied in terms of removal of Cr(VI) from water through batch experiments and UV-visible spectroscopy. The results revealed that the synthesized material has exhibited more than 97% removal capacity of Cr(VI) under optimal condition (pH 2, contact time of 90 minutes), signifying its utility as an efficient adsorbent. Therefore, ZIF-67 derived carbon composites constitute potential alternatives for treating heavy metal pollution in water sources.

Keywords*: ZIF-67, Heavy metal adsorption, MOFs, Derived Carbon, Cr(VI)*

Table of Contents

List of Figures

List of Tables

CHAPTER 1: INTRODUCTION

1.1 Background

Water is one of the most crucial materials for survival of life, sustain ecosystem as well as economic development. Agricultural sector manly consume water comprising about 70% followed by industrial sector around 20% and household use around 10%. The available freshwater for use is very limited comprising about 0.06% of water on the earth. It is estimated that water demand will increase by 19% by 2050 (Ahuja, 2015). With rapid growth of Global population, followed by industrialization, water pollution has been significantly increased. Urban wastewater is a prime carrier of conventional to emerging water pollutants such as dyes, pesticides, chemicals, pharmaceuticals and heavy metal ions.

Municipal wastewater has been one of the primary sources of water pollution especially surface water pollution. Untreated municipal wastewater contains excessive amount of dissolved organic matters which act as nutrients and can harbor pathogens responsible for outbreaking waterborne diseases (Ley et al., 2020). Excessive nutrients are also for limiting biological oxygen demand and chemical oxygen demand and foul smell (Preisner, 2020). It is one of the sources of pollution for other water sources such as lakes and rivers (Wei et al., 2024). In addition to dissolved matter, solid wastes are responsible for river pollution. Studies have shown that pollution in Bagmati river in Kathmandu valley of Nepal is due to improper management of dissolved municipal waste as well as solid waste (Ghimire et al., 2022). Municipal solid waste landfills have been reported as an underestimated source of pharmaceutical and personal care products which leach out and ultimately pollute water bodies (Yu et al., 2020).

Agriculture is the major global water consumption sector comprising about 70% of total water consumption. Almost wastewater from agricultural sectors is released untreated (Zhao & Duan, 2025). A recent statical study has reported that there is 35% and 14% enrichment of global river nitrogen and phosphorous content, respectively, by anthropogenic activities (McDowell et al., 2025). Agricultural activities such as use of synthetic fertilizers is the primary contributor. Nitrogenous and phosphate fertilizers applied to agricultural fields leach and cause groundwater contamination. Washed out fertilizers directly contaminate surface water (Zapata et al., 2023).

Nitrates and phosphates are responsible for excessive algal bloom leading direct effect on aquatic biodiversity. Pesticides are another dreadful cause of water pollution and human health (Cossu et al., 2024). In recent decades, use of veterinary items such as disinfectants, antibiotics and other animal husbandry products have appeared as emerging water pollutants(Emadi et al., 2022).

Industrial activities constitute a major source of toxic water pollutants. The textile industry releases synthetic dyes, surfactants, and heavy metals in its effluents; the metal processing and electroplating industries discharge significant quantities of toxic heavy metal ions including chromium (Cr), lead (Pb), cadmium (Cd), and nickel (Ni) (Oladimeji et al., 2024; Saratale et al., 2018) and pharmaceutical industries release biologically active compounds, solvents, and trace metals into wastewater streams(Ahmad et al., 2016). These industrial pollutants are highly persistent, toxic even at trace concentrations, and resistant to conventional wastewater treatment processes. (Bețianu et al., 2024).

According to United Nations data, approximately 80% of diseases and 50% of child deaths in developing countries are associated with contaminated water. These alarming statistics have forced urgent action toward advanced wastewater treatment and water purification technologies(Tella et al., 2025). This has driven the development of advanced materials, sustainable treatment technologies, and formulation and implementation of effective environmental policies at national and international levels.

1.2 Heavy Metals as Major Water Pollutants

Heavy metals refer to metallic substances having density greater than 5g/cm3 and generally having atomic number above 20. Unlike organic pollutants, heavy metals are not biodegradable but remain in the environment forever, they bioaccumulate within biological structures over time through the food chain and cause chronic toxicity despite being present in very small quantities(Azimi et al., 2017). The heavy metals of environmental importance as pollutants are lead (Pb), Chromium (Cr), Cadmium (Cd), Mercury (Hg), Arsenic (As), Copper (Cu), Zinc (Zn), and Nickel (Ni) (Rahman & Singh, 2019). These are classified as priority pollutants by both United States Environment Protection Agency (USEPA) and World Health Organization (WHO) due to their carcinogenicity,

mutagenicity, teratogenicity, and severe damage to the central nervous system, Kidneys, and liver(Qasem et al., 2021).

Major human-made sources of heavy metal pollution in water bodies are industrial effluents, mining and smelting activities, agricultural runoff, and municipal wastewater effluents (Briffa et al., 2020). Large amounts of Pb, Cr, Cd, and Ni are released in wastewater by industrial processes like electroplating, leather tanning, battery production, metal finishing, and pigment production (He et al., 2022). Acid mine drainage is an important source of toxic metals such as As, Hg, Cu and Zn to surrounding water bodies associated with mining(Sheoran & Sheoran, 2006). Heavy metal contamination in aquatic systems can also be caused by agricultural runoff which contains residues of pesticide and soil adsorption and by atmospheric deposition caused by industrial combustion (Nnaji et al., 2023).

Unfortunately, research has shown the levels of heavy metals in untreated industrial effluents to be several orders of magnitude higher than the maximum permissible limits set by the WHO; for As it is 0.01mg/L and for industrial effluent it is 5mg/L, for Pb it is 0.003mg/L and 3mg/L for industrial effluents, for Cd it is 0.003mg/L and 3mg/L for industrial effluents, for Cr(VI) it is 0.05mg/L and 5mg/L for industrial effluents and for Hg it is 0.006mg/L and 0.3mg/L for industrial effluents (Hanikel et al., 2020). In children, chronic exposure to high levels of Pb leads to neurological damage and developmental impairment; chronic exposure to Cd leads to renal tubular dysfunction and Itai-Itai disease; chronic exposure to high levels of As results in skin, lung and bladder cancers, and chronic exposure to high levels of Cr(VI) results in respiratory cancer (Briffa et al., 2020). The health impact of these effects is quite serious and permanent, making the need for effective technologies to remove heavy metals from contaminated water extremely critical (Rasin et al., 2025).

Table 1: Limitations of heavy metal ions

Heavy Metal ion	**Guideline Limit (WHO)**	**Health Concern**
Chromium (Cr^{6+})	0.05 mg/L	Carcinogenic, liver/ Kidney damage
Lead (Pb^{2+})	0.01 mg/L	Neurological damage, especially in children
Arsenic (As^{3+}/ As^{5+})	0.01 mg/L	Skin lessions, Cancer, cardiovascular diseases
Cadmium (Cr^{6+})	0.003 mg/L	Kidney damage, bone demineralization
Nickel (Ni^{2+})	0.07 mg/L	Skin dermatitis, respiratory issues
Copper (Cu^{2+})	2.0 mg/L	Gastrointestinal irritation
Manganese (Mn^{2+})	0.4 mg/L	Neurological effects at high levels
Zinc (Zn^{2+})	3.0 mg/L	Taste issues, low toxicity
Iron (Fe^{2+}/Fe^{3+})	0.3 mg/L	Staining, taste (not major health risk)

1.3 Methods of Removal of Heavy Metals

Various treatment technologies have been developed and applied for the removal of heavy metals from contaminated water. These methods can be broadly classified into physical, chemical, biological, and electrochemical approaches, each with distinct advantages and limitations depending on the nature, concentration, and complexity of pollutants in the wastewater(Mustapha et al., 2024).

Physical methods include membrane filtration techniques such as nanofiltration (NF), reverse osmosis (RO), and ultrafiltration (UF) (Azmi et al., 2025). These processes use semi-permeable membranes to separate dissolved heavy metal ions from water under applied pressure. Reverse osmosis has demonstrated removal efficiencies exceeding 95% for most heavy metals; however, high energy requirements, membrane fouling, and significant brine generation are major operational challenges that limit widespread deployment, particularly in resource-limited settings (Ali et al., 2023).

Chemical precipitation, coagulation-flocculation, and ion exchange are well-established chemical methods for heavy metal removal(Hussain et al., 2023). Chemical precipitation involves the addition of alkaline reagents such as lime ($Ca(OH)_2$) or sodium sulfide (Na_2S) to convert dissolved metal ions into insoluble metal hydroxides or sulfides that can be separated by sedimentation or filtration(Wang et al., 2021). Ion exchange employs synthetic resins with selective affinity for specific metal ions, offering high removal efficiency and potential for metal recovery. While effective for high-concentration wastewaters, these methods generate significant secondary sludge, require precise pH control, and incur relatively high reagent costs(Wang et al., 2021).

Biological methods, including biosorption and bioaccumulation, utilize the metal-binding capacity of microorganisms, algae, fungi, and plant biomass to sequester heavy metals from water(Nascimento et al., 2023). Biosorbents derived from agricultural waste, bacterial biomass, and algal cell walls have attracted considerable interest owing to their low cost and renewability. However, sensitivity to environmental conditions such as pH and temperature, limited mechanical stability, and difficulties in separating biosorbent from treated water have impeded large-scale application(Nnaji et al., 2023).

Electrochemical methods such as electrocoagulation, electrodeposition, and electrodialysis facilitate efficient removal of metal ions through applied electric fields(Ahalya et al., 2003). Electrocoagulation generates metal hydroxide coagulants in situ from sacrificial electrodes, simultaneously treating multiple contaminants; electrodeposition recovers dissolved metals as solid metal deposits on cathode surfaces (Peng & Guo, 2020). These methods avoid chemical reagent addition and can achieve high selectivity; however, significant energy consumption and electrode passivation over extended operation limit cost-effective scale-up(Rajoria et al., 2022).

Adsorption-based methods have emerged as among the most promising approaches for heavy metal removal due to their operational simplicity, high efficiency, design flexibility, and potential for adsorbent regeneration and reuse (Satyam & Patra, 2024). Adsorption involves the transfer of metal ions from the aqueous phase onto the surface of a solid adsorbent via physical or chemical interactions including electrostatic attraction, surface complexation, ion exchange, and chelation(Akhtar et al., 2024). Activated carbon has historically been the most widely used adsorbent; however, its high production cost and limited selectivity have motivated intensive research into alternative and advanced adsorbent materials including zeolites, clay minerals, biochar, and engineered nanomaterials(Ayach et al., 2024).

1.4 Nanomaterials for Removing Heavy Metals

Nanomaterials have attracted immense research interest in water treatment owing to their exceptionally high surface area-to-volume ratios, tunable surface chemistry, and unique physicochemical properties that differ fundamentally from those of their bulk counterparts(Wang et al., 2012). Nanomaterials with dimensions in the range of 1–100 nm exhibit quantum-mechanical effects and enhanced surface reactivity, making them highly effective for adsorptive removal of heavy metal ions even at very low concentrations(Ethaib et al., 2022). The nanoscale dimensions also enable short intraparticle diffusion distances, resulting in rapid adsorption kinetics compared to conventional adsorbents.

Commonly investigated nanomaterials for heavy metal remediation include metal oxide nanoparticles (TiO_2, Fe_3O_4, ZnO, MnO_2, Al_2O_3), zero-valent iron (ZVI) nanoparticles, layered double hydroxides (LDHs), carbon-based nanomaterials, and various nanocomposites combining

two or more functional components(Yang et al., 2019). Iron oxide nanoparticles are particularly attractive due to their superparamagnetic properties, which enable facile magnetic separation of the adsorbent from treated water using an external magnetic field, addressing one of the key practical challenges of nanomaterial-based water treatment efficient particle recovery and reuse(Singh et al., 2021). Manganese oxide nanoparticles exhibit strong oxidative affinity for As(III) and Pb^{2+}, while ZVI nanoparticles are effective reductants for Cr(VI) and As(V) immobilization(Mustapha et al., 2024).

Despite their considerable promise, several challenges must be addressed before widespread deployment of nano-adsorbents in real water treatment systems. Nanoparticle aggregation under high ionic strength conditions significantly reduces effective surface area and adsorption capacity(Singh et al., 2021). Concerns regarding potential ecotoxicity of engineered nanoparticles to aquatic organisms and their fate and transport in the environment necessitate careful risk assessment(Singh et al., 2021). Furthermore, challenges in cost-effective large-scale synthesis and the need for robust separation and regeneration strategies remain active areas of research.

1.5 Carbon Nanomaterials and Their Composites for Heavy Metal Removal

Carbon-based nanomaterials represent one of the most intensively studied classes of adsorbents for heavy metal removal from water (Hamda et al., 2025). This family encompasses carbon nanotubes (CNTs), graphene and its derivatives (graphene oxide, GO; reduced graphene oxide, rGO), fullerenes, carbon nanodots, and biochar-derived nanostructures(Yu et al., 2018). The extraordinary specific surface area, excellent chemical stability, and versatile surface functionalization capability of these materials make them superior to conventional activated carbon for trace heavy metal adsorption (Hamda et al., 2025).

Graphene oxide (GO) is a particularly attractive adsorbent owing to the abundance of oxygen-containing functional groups including carboxyl (–COOH), hydroxyl (–OH), and epoxide (–C–O–C–) moieties on its basal planes and edges (Khine et al., 2022). These groups provide a high density of active sites for coordination, complexation, and electrostatic interaction with cationic heavy metal species such as Pb^{2+}, Cu^{2+}, Cd^{2+}, and Hg^{2+}. Multi-walled carbon nanotubes (MWCNTs), when acid-functionalized, similarly exhibit high adsorption capacities for Pb^{2+}, Cd^{2+}, and Zn^{2+}, as

well as for anionic pollutants such as Cr(VI) and As(V) after surface modification(Chandran et al., 2023; Yu et al., 2018).

Nanocomposites integrating carbon nanomaterials with metal oxides, polymers (chitosan, polyaniline), or zeolites have demonstrated synergistic improvements in both adsorption capacity and selectivity compared to single-component systems. Magnetic graphene oxide composites (Fe_3O_4/GO) combine the high adsorption efficiency of graphene oxide with the superparamagnetic recoverability of iron oxide nanoparticles, significantly improving practical applicability. Chitosan-functionalized CNT composites have shown excellent performance for simultaneous removal of multiple heavy metals. Recent literature reports maximum adsorption capacities of GO-based composites exceeding 200 mg/g for Pb^{2+}, substantially outperforming most commercially available adsorbents(Chandran et al., 2023).

1.6 Jacaranda as a Sustainable Carbon Precursor

The development of sustainable, low-cost carbon precursors has become a key research priority in the synthesis of advanced carbon-based nanomaterials for environmental applications. Biomass-derived carbons offer several advantages over fossil-derived carbon sources including renewability, lower cost, reduced environmental footprint, and the ability to introduce heteroatom functional groups that enhance adsorption activity(Amin et al., 2025). Among the diverse biomass feedstocks under investigation, Jacaranda (Jacaranda *mimosifolia*) has attracted growing interest as a promising sustainable carbon precursor.

Jacaranda *mimosifolia*, the purple flowering ornamental tree species commonly seen in places like Kathmandu. It belongs to the Bignoniaceae family and is native to South America but extensively cultivated across tropical and subtropical regions worldwide. It generates substantial quantities of biomass waste in the form of seed pods, fallen leaves, and pruning residues that are typically discarded without value recovery(Amin et al., 2025). Jacaranda seed pods are like a woody fruit capsules formed after the flower matures. They are flat and round to oval shaped; brown when mature and dry; hard, lightweight, and woody; and filled with many thin, flat, winged seeds. Its lignocellulosic biomass is particularly rich in cellulose, hemicellulose, and lignin as the primary

structural polymers that serve as ideal precursors for carbonization and pyrolytic conversion to carbon-rich materials.

When jacaranda seed pods are carbonized, their organic structure breaks down and leaves behind a carbon-rich porous material having high surface area, micro-pores and meso pores, oxygen containing functional groups, carbon rich structure and has possible active sites for binding pollutants. This is the main reason for researcher to use jacaranda seed pod biochar or activated carbon to remove the pollutants from water, including heavy metals and organic contaminants (Khine et al., 2022). Subsequent chemical activation typically using KOH, $ZnCl_2$, or H_3PO_4 as activating agents can further enhance the surface area (exceeding 1000 m^2/g in optimized cases), pore volume, and surface chemistry of the resulting activated carbon(Patel et al., 2025). The inherent nitrogen and oxygen heteroatoms present in the lignocellulosic precursor are partially incorporated into the carbon framework during pyrolysis, providing additional metal coordination sites. The utilization of Jacaranda waste biomass as a carbon precursor thus simultaneously achieves waste valorization and production of a high-performance, cost-effective adsorbent material for water purification(Patel et al., 2025).

Jacaranda Seed Pods are valuable for MOF/biochar type research as it is a waste biomass usually fall from trees and are not used commercially. Their woody structure are naturally carbon rich and suitable for carbonization which produce the pores useful for the adsorption. They can be used as the scaffold for MOF-derived carbon composites, metal nanoparticles or activated carbon materials. It could be the low cost and locally available sustainable materials for research.

Figure 1: *Jacaranda Mimosifolia* with its seed pods and flower

1.7 Metal-Organic Frameworks and Derived Carbon Composites

Metal-organic frameworks (MOFs) are a class of porous crystalline hybrid materials self-assembled from metal ions or metal-oxide clusters coordinated by multidentate organic ligand linkers through strong coordination bonds (Khine et al., 2022). Their defining characteristics include ultra-high specific surface areas (up to 7000 m^2/g), precisely tunable and uniform pore sizes, extraordinarily high pore volumes, and highly versatile chemical functionality, positioning them among the most promising next-generation porous materials for adsorption applications(Xiao et al., 2023). Since their systematic development in the late 1990s, thousands of structurally distinct MOF architectures have been reported, with a growing subset demonstrated to be effective for water treatment.

For heavy metal removal from water, MOFs offer multiple and synergistic interaction mechanisms. Open metal coordination sites within the MOF framework can directly coordinate with soft Lewis-base heavy metal ions. Functional groups on the organic linkers including amino

(–NH_2), thiol (–SH), carboxylate (–COO^-), and hydroxyl (–OH) moieties provide rich chelation sites for divalent and trivalent metal cations. The uniform micropores and mesopores of MOFs can additionally confer size-selective adsorption.(Liu et al., 2018). Zeolitic imidazolate frameworks (ZIFs), particularly ZIF-8 and ZIF-67, have been widely explored owing to their excellent chemical and thermal stability and tunable nitrogen-rich framework chemistry (Jadhav et al., 2022).

MOF-derived carbon composites (MDCs) are synthesized through controlled pyrolysis of MOF precursors, yielding hierarchically porous carbon frameworks that inherit the ordered porosity of the parent MOF while acquiring the superior chemical stability and conductivity characteristic of carbon materials. The pyrolysis process affords simultaneous in situ formation of metal or metal oxide nanoparticles uniformly distributed within the carbon matrix derived from the metal nodes of the MOF providing additional active sites and enabling synergistic adsorption and reductive immobilization mechanisms for heavy metals(Ran et al., 2025). MDCs derived from ZIF-8 and ZIF-67 have demonstrated outstanding performance for removal of As (V), Cr(VI), Pb^{2+}, and Cd^{2+}, with adsorption capacities substantially exceeding those of conventional activated carbon. The integration of sustainable biomass-derived carbon with MOF-derived architectures represents a particularly compelling strategy to combine low cost, environmental sustainability, and high adsorption performance in next-generation adsorbents for water remediation(Li et al., 2018).

1.8 Problem Statement and Research Gap

Despite significant advances in nanomaterial-based adsorbents for heavy metal removal, several critical knowledge and technology gaps remain in the existing literature. First, the majority of high-performance adsorbents reported to date rely on expensive, non-renewable precursors and complex multi-step synthesis procedures, fundamentally limiting their scalability and economic viability for real-world water treatment applications, particularly in low- and middle-income countries where heavy metal contamination is most acute.

Second, while MOF-derived carbon composites have demonstrated excellent heavy metal removal performance, the potential of sustainable, renewable biomass-derived carbon precursors such as Jacaranda waste biomass for the synthesis of MOF-carbon composites has been insufficiently

explored. Such an approach could substantially reduce synthesis costs while maintaining high performance and aligning with green chemistry principles.

Third, the simultaneous removal of multiple co-existing heavy metal contaminants (e.g., Pb^{2+}, Cd^{2+}, Cr(VI), and As(V)) from complex, multi-component wastewater matrices remains a significant challenge. The large majority of published studies evaluate single-metal systems under idealized laboratory conditions, which do not adequately reflect the competitive adsorption dynamics in real industrial and municipal effluents containing multiple co-contaminants.

Fourth, the long-term reusability and regeneration performance of advanced adsorbents across multiple adsorption-desorption cycles, a critical requirement for practical and economically viable application is rarely comprehensively evaluated in published literature. Accordingly, there is a pressing need to develop sustainable, cost-effective, and high-performance Jacaranda-derived carbon-MOF composite adsorbents and rigorously evaluate their performance for multi-metal removal under environmentally relevant conditions.

1.9 Research Objectives

1.9.1 General Objective

The general objective of this study is to synthesize and evaluate a Jacaranda seed pod biomass–based metal–organic framework (MOF)-derived carbon composite for the efficient removal of heavy metal ions like Cr(VI) from aqueous systems, with a focus on developing a low-cost, sustainable, and high-performance adsorbent.

1.9.2 Specific Objectives

To achieve the above general objective, the following specific objectives are proposed:

- To prepare Jacaranda seed pod biomass through appropriate cleaning, drying, and size reduction processes for use as a substrate material.

- To synthesize MOF (e.g., ZIF-67) on the biomass surface via in-situ growth techniques to form a JSP–MOF composite.

- To characterize the prepared materials using analytical techniques such as FTIR, SEM-EDX, and other relevant methods to determine surface morphology, functional groups, and elemental composition.

- To investigate the adsorption performance of the prepared composite for the removal of heavy metal ions (e.g., Cr(VI)) from aqueous solutions.

- To analyze the adsorption mechanism using appropriate models (e.g., adsorption isotherms and kinetics) and evaluate possible reduction processes (e.g., Cr(VI) to Cr (III)).

CHAPTER 2: LITERATURE REVIEW

2.1 Overview of Heavy Metal Removal Techniques

Heavy metal contamination in water has become a major environmental concern due to the toxic, persistent, and non-biodegradable nature of metals such as chromium (Cr), lead (Pb), cadmium (Cd), arsenic (As), and mercury (Hg)(Singh et al., 2022). These metals are introduced into aquatic systems through industrial Processes like electroplating, battery production, mining, leather tanning, and inappropriate waste disposal (Wang & Wang, 2025). Once released into the environment, heavy metals do not degrade and can accumulate in living organisms, leading to bioaccumulation and biomagnification. They can bring a serious health issues, like neurological abnormalities, and cancer even at extremely low quantities. So, it is difficult to remove heavy metals from wastewater to protect both human health and the environment (Jagaba et al., 2024).

Several treatment methods have been developed to eliminate the heavy metals from water, such as physical, chemical, and biological methods (Kikuchi & Tanaka, 2012). Chemical precipitation is one of the most commonly used methods in industrial applications, where chemicals such as lime or sodium hydroxide are added to convert dissolved metal ions into insoluble compounds(Sharma et al., 2025). Although this method is simple and effective for high metal concentrations, it generates large amounts of sludge and is less efficient for dilute solutions. Ion exchange is another widely used technique, where metal ions are replaced with less harmful ions using synthetic resins. This method is highly selective but relatively expensive and requires regeneration(Mishra et al., 2018).

Membrane-based processes, such as and ultrafiltration, nanofiltration, and reverse osmosis, have also been employed for heavy metal removal (Castro & Abejón, 2024). These methods provide high removal efficiency by physically separating metal ions from water through semi-permeable membranes. However, their high operational cost and issues such as membrane fouling limit their widespread use. Biological methods, including biosorption and bioaccumulation using microorganisms, have gained attention as eco-friendly alternatives. However, these methods are generally slower and sensitive to environmental conditions(Munir et al., 2021).

Adsorption has been recognized as one of the most effective and promising methods for heavy metal removal than other techniques because of its simplicity, high efficiency, and ability to treat low concentrations of contaminants (Raji et al., 2023). The effectiveness of adsorption depends largely on the properties of the adsorbent material, which has led to extensive research on the development of advanced adsorbents(Sharma et al., 2025).

2.2 Adsorbent Materials for Heavy Metal Removal

Various adsorbent materials have been studied for the removal of heavy metals from aqueous systems. Among them, activated carbon is the most commonly used adsorbents due to its high surface area, well-developed porosity, and strong adsorption capacity (Ganjoo et al., 2023). It can effectively remove a wide range of contaminants, including heavy metal ions (Darban et al., 2022). However, it has a high production cost which become its limitation for its wide application.

Natural materials such as clays and zeolites have also been excessively used because of its availability and minimum cost. These materials possess ion-exchange properties and can remove metal ions through electrostatic interactions and ion exchange mechanisms. However, their adsorption capacity is generally lower compared to advanced materials(Topare & Wadgaonkar, 2023).

Polymer-based adsorbents and ion-exchange resins offer high selectivity and efficiency for specific metal ions. These materials can be designed with functional groups that selectively bind to target contaminants(Chakraborty et al., 2022; Rafi, 2018). Despite their effectiveness, they are often expensive and may not be environmentally sustainable.

In recent years, nanomaterials have emerged as highly promising adsorbents due to their extremely small particle size and large surface area (Sadegh et al., 2017). Materials such as graphene oxide, carbon nanotubes, and metal oxide nanoparticles exhibit enhanced adsorption capacity and can also participate in redox reactions (Wang & Chen, 2015). For example, iron-based nanoparticles can reduce toxic Cr(VI) to Cr(III). However, challenges such as high cost, potential toxicity, and difficulty in recovery after use need to be addressed(Hamadneh et al., 2026; Rafi, 2018).

2.3 Metal-Organic Frameworks (MOFs) in Water Treatment

Metal-organic frameworks (MOFs) represent a recent class of porous hybrid materials that have attracted considerable research interest for environmental applications (Chongdar et al., 2022). They are composed of metal ions or clusters linked by organic ligands, forms highly ordered three-dimensional poros architectures with exceptionally large surface areas and tunable pore sizes (Chongdar et al., 2022). These unique properties make MOFs highly suitable for adsorption applications (Motshekga et al., 2024).

In heavy metal removal, MOFs provide numerous active sites for binding metal ions and allow efficient diffusion through their porous structure. The chemical functionality of MOFs can also be modified to enhance their selectivity toward specific metal ions. Among various types of MOFs, zeolitic imidazolate frameworks (ZIFs), such as ZIF-67, are particularly important due to their high thermal stability and resistance to chemical degradation(Kumar et al., 2018).

However, the practical application of MOFs in water treatment is limited by several factors. Many MOFs exhibit poor stability in aqueous environments, leading to structural degradation. Additionally, the recovery and reuse of MOF particles can be challenging, and their synthesis can be relatively expensive. These limitations have driven research toward the development of modified and derived materials(Rastin et al., 2025).

2.4 MOF-Derived Carbon Materials

To overcome the limitations associated with pure MOFs, researchers have developed MOF-derived carbon materials through thermal treatment processes such as pyrolysis or carbonization under inert atmospheres (Ren et al., 2020) . During this process, the organic ligands decompose to form a carbon matrix, while the metal ions are converted into metal or metal oxide nanoparticles embedded within the carbon structure (Chai et al., 2025).

These MOF-derived carbon materials retain the porous structure of the original MOF while exhibiting improved thermal stability, chemical resistance, and electrical conductivity. The presence of heteroatoms such as nitrogen within the carbon framework further enhances adsorption

performance by providing additional active sites (Ding et al., 2022). Moreover, the embedded metal nanoparticles can act as catalytic centers, enabling redox reactions in addition to adsorption.

For heavy metal removal, MOF-derived carbons offer significant advantages. They not only adsorb metal ions effectively but can also transform them into less toxic forms(Sundararaman et al., 2025) . For example, Cr(VI) can be reduced to Cr (III), which is less harmful and easier to remove from water. This dual functionality makes MOF-derived carbon materials highly attractive for advanced water treatment applications.

2.5 Biomass-Based Adsorbents and Sustainable Materials

The increasing demand for sustainable and low-cost water treatment solutions has led to growing interest in biomass-based adsorbents. These materials are derived from natural sources such as agricultural waste, plant residues, and other renewable resources(Zhang et al., 2023). Examples include rice husk, coconut shell, sawdust, and seed pods.

Biomass materials contain various functional groups such as hydroxyl, carboxyl, and amino groups, which can interact with heavy metal ions through different mechanisms(Aragaw & Bogale, 2021). Additionally, biomass can be converted into biochar through thermal treatment, resulting in a porous carbon material with improved adsorption properties.

Biomass-based adsorbents are environmentally friendly, biodegradable, and cost-effective (Shree et al., 2025). They also contribute to waste management and resource recycling. However, their adsorption capacity and mechanical stability are often lower compared to advanced materials, which limits their performance in practical applications.

2.6 Biomass-MOF Composite Materials

To enhance the performance of biomass-based adsorbents, researchers have developed composite materials by combining biomass with MOFs. In these composites, biomass serves as a support material and carbon source, while MOFs provide high surface area and well-defined porous structures (Jiang et al., 2024).

The in-situ growth of MOFs on biomass surfaces allows for uniform distribution and strong interaction between the two components. This prevents aggregation of MOF particles and improves the stability of the composite. Upon carbonization, these composites are transformed into biomass–MOF-derived carbon materials with hierarchical porosity and enhanced surface properties(Jiang et al., 2024).

Such composite materials exhibit improved adsorption capacity, better stability, and additional functionalities compared to individual components. The presence of metal nanoparticles within the carbon matrix further enhances catalytic activity, particularly for redox-based removal processes(Li et al., 2025). As a result, biomass–MOF composites have shown great potential for efficient heavy metal removal(Li et al., 2025).

JSP-MOF900 was compared to other adsorbents reported earlier for the Cr(VI) removal, as listed in Table 4. While some of the adsorbents made from ZIF-67 showed better adsorption capacity, the JSP-MOF900 composite shows comparatively high adsorption efficiency of 97.75% even under acidic conditions and short contact time. This level of adsorption efficiency is greater than many biomass-based adsorbents and equal to others based on nitrogen-doped carbons. The variation in the adsorption capacity can be due to differences in parameters such as the concentration of solution, pH, and adsorption model used in various studies. Even though the JSP-MOF900 adsorbent does not have a very high adsorption capacity, it is advantageous because of the use of cost-effective biomass and easy preparation method.

Table 2: Comparison of Absorption of Cr(VI) of JSP-MOF900 with previous reported Absorbents

Absorbent	**Adsorption Capacity / Removal Efficiency**	**Conditions**	**Authors (Year)**
ZIF-67 derived magnetic nanoporous carbon coated by poly(m-phenylenediamine) (MNC@PmPD)(Gao et al., 2021)	240.44 mg/g	Acidic pH, batch	Gao et al. (2021)
ZIF-67 nanocrystals for $Cr_2O_7^{2-}$ removal	370 mg/g	Batch, Langmuir model	Abdelhameed et al. (2023)
Magnetic Fe_3O_4/ZIF-67@Aminated Chitosan composite beads(Omer et al., 2021)	119.05 mg/g	pH 2, 25°C, batch	Omer et al. (2021)
Biosorbent derived from *Arundo donax* stem (CADSP)(Bhattarai et al., 2022)	76.92 mg/g	pH 2, batch	Bhattarai et al. (2022)
N-doped porous carbon from bamboo shoots (Qu et al., 2024)	>90% removal	Acidic pH, batch	Chen et al. (2024)
JSP-MOF900 — ZIF-67 derived carbon from Jacaranda seed pods (This study)	**97.75%**	**pH 2, 90 min, batch**	**This work**

CHAPTER 3: MATERIALS AND METHODS

3.1 Overview of Experimental Design

This study involved a multi-step experimental approach encompassing: (i) preparation and characterization of Jacaranda seed pod (JSP) substrate, (ii) in-situ growth of ZIF-67 onto the JSP substrate in aqueous medium, (iii) controlled carbonization at three different temperatures to produce MOF-derived carbon composites, (iv) physicochemical characterization of all synthesized materials, and (v) evaluation of adsorption performance for hexavalent chromium [Cr(VI)] removal from simulated wastewater. The study was conducted at the laboratory facilities of Pulchowk Campus, Institute of Engineering, Tribhuvan University, Nepal.

3.2 Materials and Reagents

Cobalt nitrate hexahydrate ($Co(NO_3)_2 \cdot 6H_2O$, ≥98%, Junsei Chemical Co. Ltd) and 2-methylimidazole (2-MeIM, ≥98%, Sigma- Aldrich) were used as the cobalt metal precursor and organic ligand, respectively, for ZIF-67 synthesis. Cobalt chloride hexahydrate and 2-methylimidazole can be successfully coordinated in methanol solvent at ambient temperature to produce ZIF-67 with a sodalite-type framework. Potassium dichromate ($K_2Cr_2O_7$, ≥99%, Qualigens) was used as the source of Cr(VI) for preparing stock and working solutions. Dilute nitric acid (HNO_3, 0.1 N) was used as the solvent for the Cr(VI) stock solution, and distilled water was used for pH adjustment. Diphenylcarbazide (DPC, ≥98.5%, ChemSynth) is used as a coloring agent. All the chemicals used in laboratory were analytical reagent (AR) grade. Distilled water was used throughout all synthesis and adsorption experiments.

Jacaranda Mimosifolia seed pods were collected locally and used as the natural biomass substrate. Biomass is an ideal substrate for loading MOFs due to its abundance, mechanical properties, low cost, high porosity, and low density and MOF crystals can be anchored on biomass surfaces through physical adsorption, hydrogen bonding, or chemical bonding with hydroxyl groups (Zou et al., 2024).

3.3 Preparation of Jacaranda Seed Pod (JSP) Substrate

Jacaranda seed pods were washed with distilled water to remove surface dust and impurities. The washed pods were then dried in an oven at 80 °C for 24 hours to eliminate moisture. The dried pods were ground using a mechanical grinder and sieved to obtain a uniform fine powder. The resulting powder was designated as JSP-Pristine and served as the base substrate for ZIF-67 growth (Mukhiya et al., 2021).

3.4 In-situ Growth of ZIF67 on JSP

ZIF-67 MOF was successfully synthesized on the surface of the Jacaranda seed pod biomass via in-situ growth technique. Initially, 8.73g of $Co(NO_3)_2 \cdot 6H_2O$ was taken in a conical flask and dissolved in 200 ml of methanol to obtain Co^{2+} ions (Mukhiya et al., 2021) . The biomass was then dispersed in the metal solution with continuous stirring to facilitate the binding of Co^{2+} ions on the surface through interaction with functional groups like hydroxyl and carboxyl groups. Subsequently, 9.85g of 2-methylimidazole was dissolved in 200 ml of methanol in separate beaker to prepare ligand solution. The JSP power was then added to metal ion solution and stirred for 3h to facilitate the interaction of metal ions with the surface of JSP particles. Then the ligand solution was slowly added to the reaction mixture under continuous stirring, and the mixture was left undisturbed for 24 h at room temperature (Mukhiya et al., 2021). The ligand bound to the Co^{2+} ions adsorbed on the surface of the biomass, which facilitated nucleation and formation of ZIF-67 crystals on the biomass surface. The appearance of a characteristic purple color confirmed the formation of ZIF-67 MOF on JSP surface. Afterward, the product was filtered, extensively washed with methanol and distilled water to eliminate all unreacted compounds and then centrifuged at 8000rpm for 7 min and dried at 80°C for 16 h in oven (Mukhiya et al., 2021) .

3.5 Carbonization and Preparation of MOF-Derived Carbon Composites

The ZIF-67/JSP composite was carbonized in a horizontal tube furnace (Kejia Furnace) under a continuous flow of nitrogen (N_2) gas to maintain an inert atmosphere and prevent oxidation during the thermal treatment (Karki, 2025). During carbonization of biomass under an inert atmosphere, several reactions occur including dehydration, decarboxylation, depolymerization, isomerization,

and aromatization and plant-based biomasses can generally retain their original structural morphology through pyrolysis.

The ZIF-67/JSP composite was placed in boat and loaded into the tube furnace. The carbonization was carried out upon three temperature 700 °C, 800 °C, and 900 °C, and held at each target temperature for 5 hours. After completion, the furnace was cooled naturally to room temperature with continuous passing of N_2 gas for prevention of re-oxidation of the material (Karki, 2025). During MOF pyrolysis in an inert atmosphere, organic linkers undergo carbonization while the metal nodes are reduced to metallic or oxide nanoparticles dispersed within the resulting porous carbon matrix, yielding MOF-derived carbon composites with high surface area and abundant active sites(Ronsse et al., 2015).

The three carbon composites obtained were designated as follows:

- JSP-MOF-700 - carbonized at 700 °C
- JSP-MOF-800 - carbonized at 800 °C
- JSP-MOF-900 - carbonized at 900 °C

All three composites, along with JSP-Pristine, were kept in sealed vials under dry conditions for further characterization and adsorption experiments.

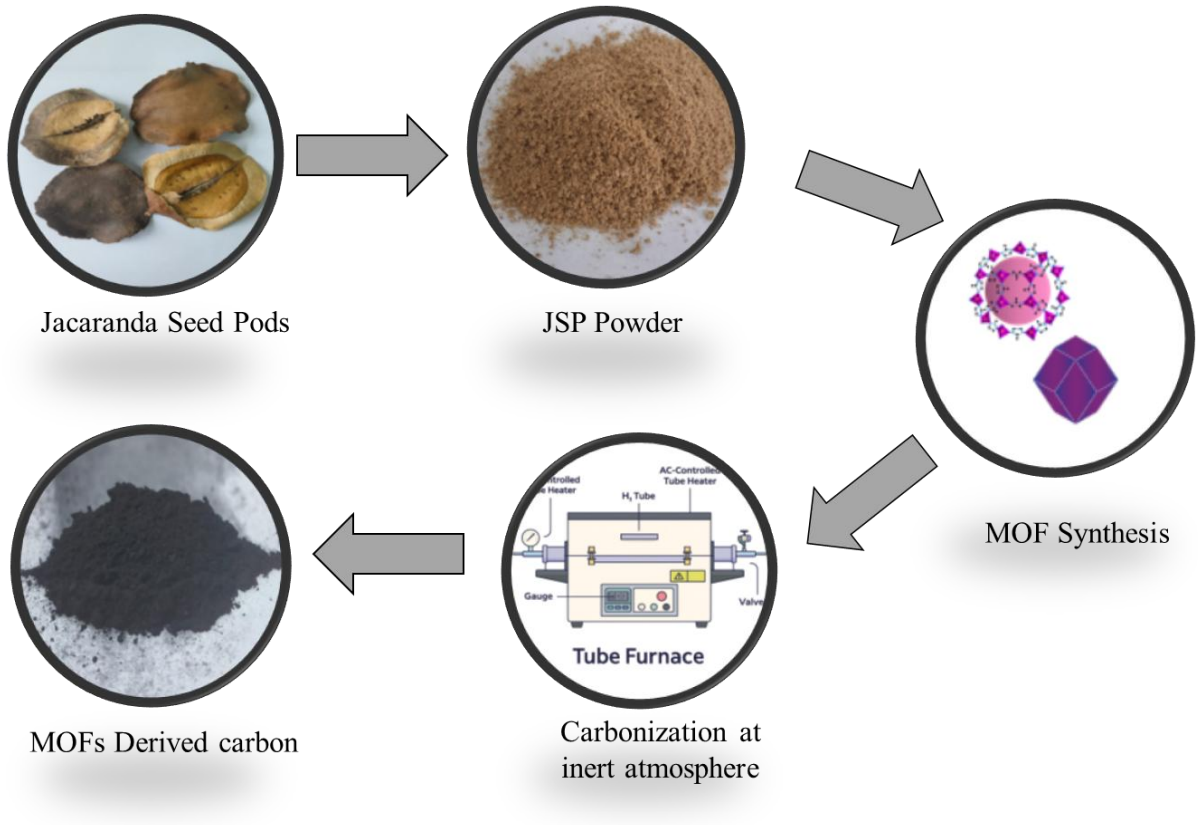

Figure 2: Schematic diagram of sample preparation

3.6 Characterization of Synthesized Materials

3.6.1 Field Emission Scanning Electron Microscopy (FESEM) and Energy Dispersive X-ray Analysis (EDX)

The surface morphology and microstructural features of JSP-Pristine, and the three carbonized composites (JSP-MOF700, JSP-MOF800, and JSP-MOF900) were examined using Field Emission Scanning Electron Microscopy (FESEM, JEOL JSM). FESEM provides high-resolution imaging of surface texture, particle size distribution, and morphological changes induced by MOF growth and subsequent carbonization. Energy Dispersive X-ray (EDX) analysis was to determine the elemental composition of the materials, confirming the presence of carbon (C), nitrogen (N), oxygen (O), and cobalt (Co) in the synthesized composites. FESEM and EDX characterization

provide critical information on the morphology, particle size, and elemental composition of ZIF-67-derived materials, offering direct evidence of successful synthesis and structural transformation upon carbonization.

3.6.2 Fourier Transform Infrared Spectroscopy

Fourier Transform Infrared Spectroscopy (FTIR) (FTIR, PerkinElmer Spectrum IR version 10.6.2) was used to identify the functional groups present on the surface of JSP-Pristine, and the MOF-derived carbon composites at Chemistry Laboratory, Amrit campus. Spectra were recorded in the wavenumber range of 400–4000 cm^{-1}. FTIR analysis of ZIF-67 shows a characteristic sharp absorption band at approximately 423 cm^{-1} due to Co–N stretching vibration, confirming bond formation between cobalt and the 2-methylimidazole ligand; additional peaks in the 995–1145 cm^{-1} region are attributed to C–N bending and stretching vibrations of the imidazolate ring (Mohamed et al., 2017). Changes in FTIR spectra across the series of materials were used to track the progressive transformation of functional groups from the pristine biomass substrate through ZIF-67 formation to the final carbonized composites.

3.7 Preparation of Cr(VI) Working Solutions

A stock solution of Cr(VI) was prepared by dissolving a precisely weighed quantity of potassium dichromate ($K_2Cr_2O_7$) in 0.1 N HNO_3. Working solutions of 10ppm concentrations were prepared by serial dilution of the stock solution using 0.1 N HNO_3. The pH of all working solutions was adjusted to pH 2 using distilled water and verified using a calibrated digital pH meter. The selection of pH 2 was based on the well-established understanding that acidic conditions favor electrostatic attraction between the positively charged adsorbent surface and the negatively charged Cr(VI) oxyanion species ($HCrO_4^-$ and $Cr_2O_7^{2-}$), which predominate at low pH values. The concentration of Cr(VI) in all solutions was determined using the standard diphenylcarbazide colorimetric method at a wavelength of 540 nm using a UV-Vis spectrophotometer.

3.8 Batch Adsorption Experiments

Batch adsorption experiments were conducted to evaluate the Cr(VI) removal performance of JSP-Pristine, JSP-MOF-700, JSP-MOF-800, and JSP-MOF-900. A 25mg of adsorbent was added to a

50 ml volume of Cr(VI) working solution in beaker and stirred by using a magnetic stirrer. The Contact time was taken as a 15, 30, 60 and 90 minutes. And the liquid sample of every subsequent contact time was taken, then it was centrifuged at 8000 rpm for 7 minutes and measured using UV-Vis spectrophotometry after adding few drops 1,5-diphenylcarbazide (DPC) solution, in the ratio 1:10 as complexing agent on it. And the adsorption was observed through UV-Vis spectrophotometry. The removal efficiency (%) was calculated as:

$$Removal\ efficiencey(\%) = \left(\frac{C_0 - Ce}{C_0}\right) * 100 \ldots\ldots\ldots\ldots\ldots\ldots\ldots\ldots (1)$$

where C_0 is the initial Cr(VI) concentration (mg/L) and Ce is the equilibrium concentration (mg/L) after adsorption. The effects of key parameters including adsorbent dosage, initial Cr(VI) concentration, contact time, and pH on removal efficiency were systematically investigated to identify optimum adsorption conditions.

3.9 Adsorption Isotherm and Kinetics

Kinetic models such as pseudo-first-order and pseudo-second-order were applied to determine the rate-controlling steps of the adsorption process.

3.9.1 Pseudo-First-Order Kinetic Model

The pseudo-first-order (PFO) kinetic model, originally proposed by Lagergren (1898), is one of the earliest and most commonly employed models for describing the rate of adsorption from a liquid phase onto a solid surface. The model has assumption that rate of adsorption at any time is directly proportional to the difference between the equilibrium adsorption capacity and the amount of adsorbate taken up at that time. Mathematically, the PFO model is expressed as:

$$dqt/dt = k_1(qe - qt) \ldots\ldots\ldots\ldots\ldots\ldots\ldots\ldots\ldots\ldots (2)$$

where qt (mg/g) is the amount of adsorbate adsorbed per unit mass of adsorbent at time t (min), qe (mg/g) is the equilibrium adsorption capacity, and k_1 (min^{-1}) is the pseudo-first-order rate constant. Integrating the above expression with the boundary condition $q_t = 0$ at $t = 0$ yields the linearized form:

$$ln(qe - qt) = ln(qe) - k_1 t \ldots\ldots\ldots\ldots\ldots\ldots\ldots\ldots\ldots\ldots (3)$$

A plot of $\ln(q_e - q_t)$ versus t gives a straight line with slope $-k_1$ and intercept $\ln(q_e)$, from which the rate constant and theoretical equilibrium capacity can be determined. The PFO model is generally applicable when the concentration of the adsorbate in solution is relatively low, or when physisorption governs the overall adsorption process. A high R^2 value (close to 1.0) from linear regression of this plot confirms the validity of the PFO model for a given adsorbent–adsorbate system.

3.9.2 Pseudo-Second-Order Kinetic Model

The pseudo-second-order (PSO) kinetic model, introduced by Ho and McKay (1999), assumes that the overall rate of adsorption is controlled by a chemisorption mechanism involving valence forces through the sharing or exchange of electrons between the adsorbent and the adsorbate. Unlike the PFO model, the PSO model assumes that adsorption involves the formation of chemical bonds and that the rate is proportional to the square of the number of unoccupied active surface sites. The differential form of the PSO model is:

$$dqt/dt = k_2(qe - qt)^2 \ldots\ldots\ldots\ldots\ldots\ldots\ldots\ldots\ldots\ldots (4)$$

where k_2 (g/mg·min) is the pseudo-second-order rate constant. Integration of this expression with the boundary condition qt = 0 at t = 0 and rearrangement yields the following linearized form:

$$t/qt = 1/(k_2 qe^2) + (1/qe)t \ldots\ldots\ldots\ldots\ldots\ldots (5)$$

A linear plot of t/q_t versus t yields a slope of $1/q_e$ and an intercept of $1/(k_2 q_e^2)$, allowing the determination of both the equilibrium adsorption capacity and the rate constant. The PSO model has been widely used in adsorption studies and is especially appropriate when chemisorption is the rate-limiting step. A higher R^2 value for PSO compared to PFO indicates that the adsorption mechanism is predominantly governed by chemical interactions rather than physical diffusion.

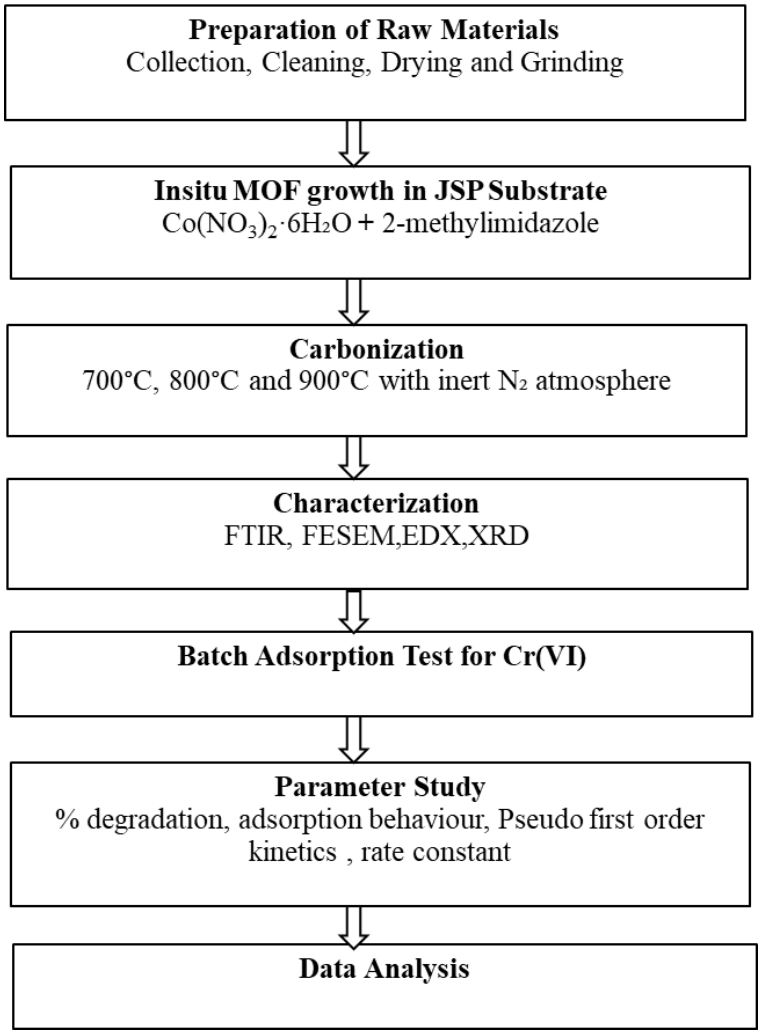

Figure 3: Research Flow Chart

CHAPTER 4: RESULTS AND DISCUSSION

4.1 Fourier Transform Infrared Spectroscopy Analysis

Fourier Transform Infrared Spectroscopy (FTIR) spectroscopy was used to investigate the evolution of surface functional groups across the JSP-derived material series. The spectra, recorded in the 4000–400 cm^{-1} range, are presented comparatively for JSP-Pristine, JSP-MOF700, JSP-MOF800, and JSP-MOF900 as shown in figure 4.

The pristine Jacaranda seed pod (JSP-Pristine) exhibited a characteristic lignocellulosic FTIR fingerprint. A broad, prominent absorption band centered around 3300–3400 cm^{-1} is attributed to O–H stretching vibrations from hydroxyl groups in cellulose and hemicellulose, as well as adsorbed moisture(Azeez & Shenbagaraman, 2025). Aliphatic C–H stretching modes appear as a doublet at approximately 2920 and 2850 cm^{-1}, corresponding to asymmetric and symmetric stretches of CH_2 and CH_3 groups present in the lignocellulosic organic structure(Kundu et al., 2023). Absorption bands in the 1600–1650 cm^{-1} region are ascribed to C=O stretching and C=C aromatic ring vibrations characteristic of lignin moieties, while the strong, complex absorption envelope in the 900–1200 cm^{-1} region corresponds to C–O–C glycosidic and ether linkages in cellulose and hemicellulose. This pattern is fully consistent with the known FTIR signatures of lignocellulosic biomass materials(Md Salim et al., 2021) (El-Azazy et al., 2022)

Upon carbonization, a systematic and progressive transformation of the FTIR spectra was observed across the JSP-MOF700, JSP-MOF800, and JSP-MOF900 series. The broad O–H stretching band (3300–3400 cm^{-1}) and aliphatic C–H stretches (2920–2850 cm^{-1}) progressively diminished with increasing carbonization temperature, reflecting the thermally driven dehydration and deoxygenation of the organic biomass matrix(Yusuf, 2023). The C–O–C glycosidic linkages in the 900–1200 cm^{-1} region similarly weakened, consistent with the decomposition of polysaccharide chains at elevated temperatures (Zhou et al., 2017). These observations collectively confirm the progressive transition from an oxygenated, aliphatic organic biomass structure to a more condensed, aromatic carbon framework with increasing carbonization temperature.

Importantly, C=N stretching vibrations, attributable to nitrogen incorporated from the 2-methylimidazole linkers of ZIF-67, were retained in the carbonized samples, confirming successful nitrogen doping within the carbon matrix(Shao et al., 2021). The emergence of new absorption features in the 500–700 cm^{-1} fingerprint region in the carbonized samples particularly in JSP-MOF800 and JSP-MOF900 is attributed to Co–N and Co–O vibrational modes, providing direct spectroscopic evidence of cobalt species incorporation derived from the ZIF-67 precursor(Yang et al., 2024). JSP-MOF900 exhibited a near-complete loss of oxygenated functional group bands, indicating the highest degree of graphitization among the three carbonized samples. A distinct absorption dip around 3000 cm^{-1} observed in JSP-MOF900 may be attributed to residual N–H stretching or C≡N contributions from nitrogen species incorporated at high temperature(Zhou et al., 2017).

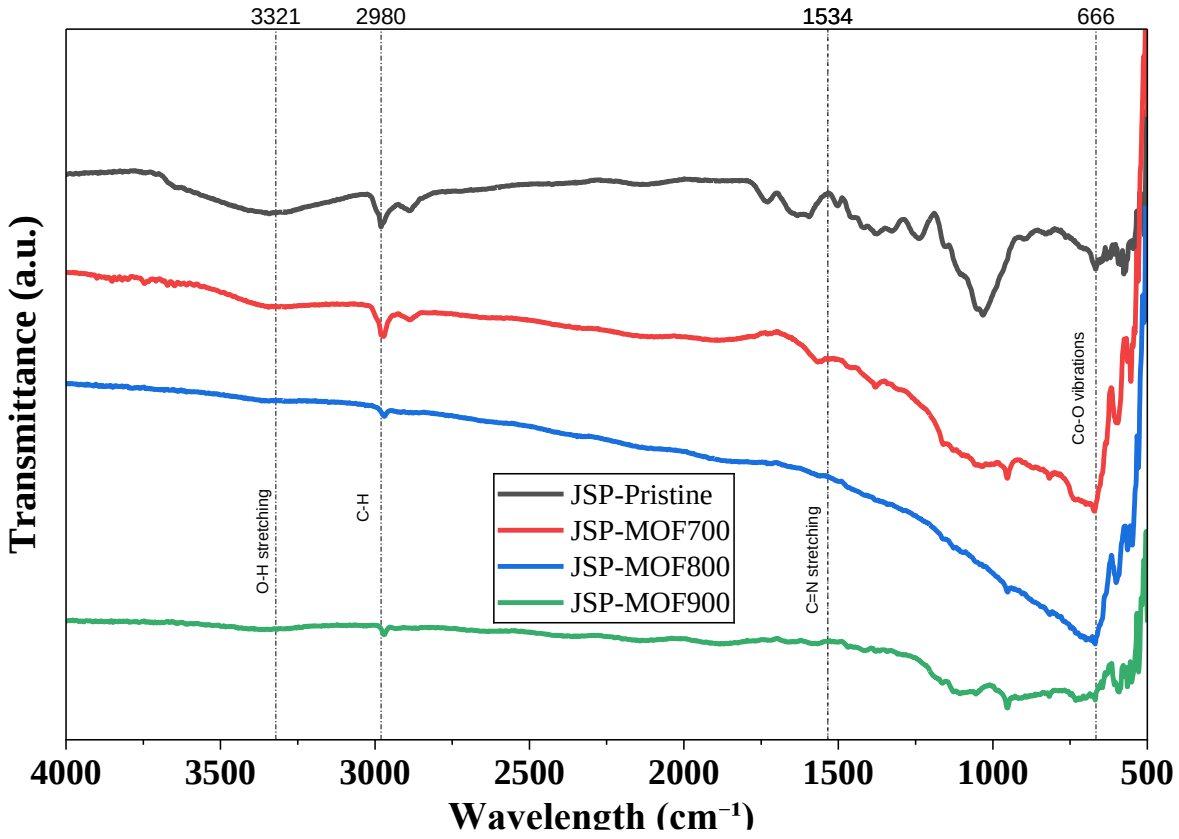

Figure 4: FTIR spectrum of powdered jacaranda seed pods and its derived carbons

4.2 FESEM Morphological Analysis

FESEM analysis provided detailed insights into the morphological evolution of the JSP-derived materials across the carbonization temperature series. Representative FESEM images were obtained at multiple magnifications (scale bars: 3 μm, 1 μm, 2 μm, 200 nm, 100 nm) to capture structural features at both the microscale and nanoscale levels.

4.2.1 JSP-Pristine (Panels a, b)

The pristine Jacaranda seed pod exhibited a characteristic layered, sheet-like architecture with irregular folding, consistent with the lamellar structure of plant cell walls. At the 3 μm scale (Panel a), macropores resulting from the natural vascular and cellular structure of the seed pod were clearly visible as pit-like features distributed across the surface. At higher magnification (1 μm, Panel b), the surface appeared relatively smooth and dense at the nanoscale, with small circular features (~100–200 nm) likely corresponding to natural stomata or pit membrane remnants. The absence of nanoparticles or defined crystal structures on this surface confirmed that the pristine biomass possesses natural microporosity but negligible nano porosity which is consistent with the FTIR-confirmed lignocellulosic composition of the unmodified material.

4.2.2 JSP-MOF700 (Panels c, d)

Carbonization at 700°C resulted in a dramatic morphological transformation from the smooth, layered pristine biomass. At the 2 μm scale (Panel c), the surface exhibited significant fragmentation and granular irregularity, with the collapse of the biomass lamellar structure and the emergence of bright, loosely aggregated clusters. At 200 nm magnification (Panel d), these clusters resolved into fluffy, cauliflower-like nano-aggregates characteristic of incipient Co nanoparticle nucleation within a partially graphitized carbon matrix. The aggregates appeared loosely packed with considerable inter-particle space, suggesting high inter-particle porosity. The incomplete carbonization at 700°C is evidenced by the disordered, non-uniform nature of the particle distribution, indicating early-stage decomposition of the ZIF-67 framework and onset of Co species nucleation.

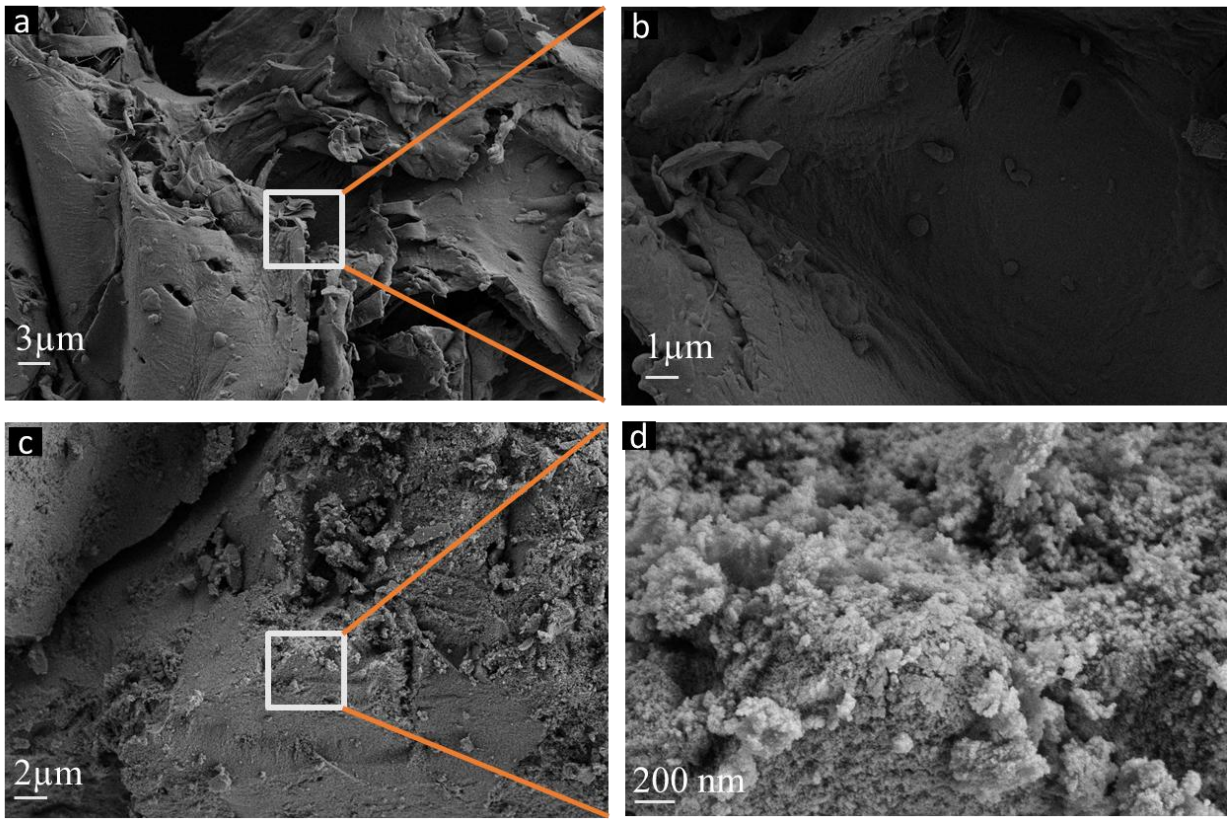

Figure 5: FESEM images of a &b) JSP-Pristine and c & d) JSP-MOF700

4.2.3 JSP-MOF800 (Panels e, f)

Carbonization at 800°C yielded a notably more consolidated and uniform morphology. At 1 µm (Panel e), the carbon sheet structure remained discernible but was now densely decorated with uniformly distributed nanoparticles, with a distinct mesopore (~300–400 nm) visible on the surface confirming pore development. At the highest magnification of 100 nm (Panel f), the material revealed a remarkably homogeneous distribution of fine Co nanoparticles (~10–20 nm) anchored firmly on the consolidated carbon matrix, with minimal agglomeration. This exceptional nanoparticle dispersion represents the defining morphological characteristic of JSP-MOF800 and is directly correlated with its superior adsorption performance, as the uniform distribution maximizes the density of accessible active sites on the material surface.

4.2.4 JSP-MOF900 (Panels g, h)

At 900 °C, FESEM images revealed a surface almost entirely covered by densely packed, well-defined spherical Co nanoparticles. At 200 nm magnification (Panel h), the particles exhibited clear spherical morphology with significant size variation, with larger particles (~100–150 nm) coexisting alongside smaller ones (~30–50 nm). This bimodal size distribution is consistent with Ostwald ripening a thermodynamically driven particle coarsening process in which larger particles grow at the expense of smaller ones under the high thermal energy provided at 900 °C. While the particle coverage on the carbon surface was visually dense, the increased particle size and evidence of sintering suggest a net reduction in accessible surface area and active site density compared to JSP-MOF800, consistent with the observed lower adsorption performance of this material.

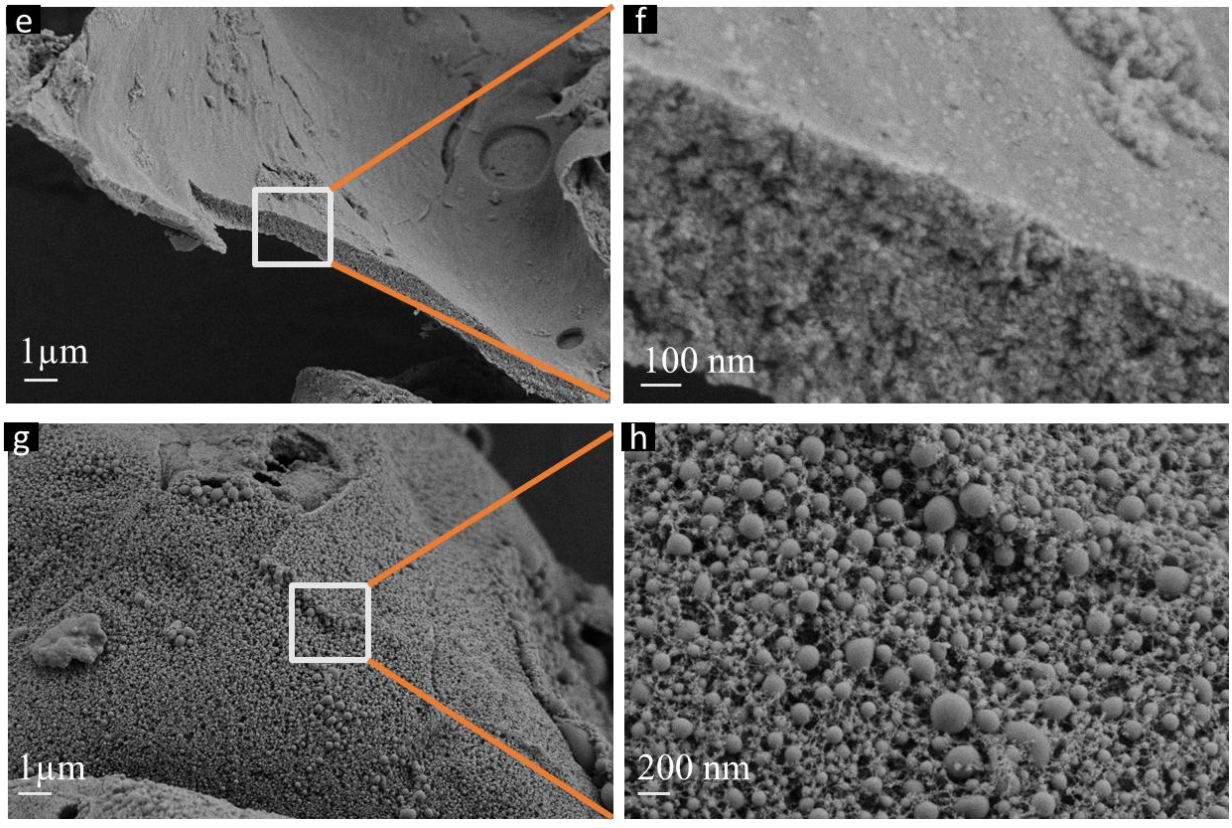

Figure 6: FESEM images of e &f) JSP-MOF800 and g & h) JSP-MOF900

4.3 EDX Analysis

The surface morphology and elemental composition of the synthesized JSP-MOF900 composite were examined using FESEM coupled with EDX spectroscopy. The FESEM micrograph revealed a flat, layered surface morphology with irregular edges at a scale of 2.5 μm, which is a typical characteristic of biomass-derived carbon materials following high-temperature carbonization. The platelet-like structure suggests that the Jacaranda seed pod substrate retained partial morphological features of the original lignocellulosic architecture even after pyrolysis, consistent with the well-established behavior of plant-based biomass during thermal treatment (Li et al., 2023).

Carbon was the dominant element at 68.27 wt%, confirming successful carbonization of both the JSP biomass substrate and the ZIF-67 organic linker. The substantial oxygen content (19.27 wt%) indicates the retention of surface functional groups such as hydroxyl (–OH), carboxyl (–COOH), and carbonyl (C=O) groups, which are known to play an active role in heavy metal adsorption through surface complexation and ion exchange (Devi et al., 2023). Cobalt was retained at 12.22 wt%, confirming that Co^{2+} nodes from ZIF-67 were successfully converted to cobalt nanoparticles embedded within the carbon matrix during carbonization, a transformation well documented in ZIF-67-derived carbon composites (Naghdi et al., 2024). Nitrogen was detected at 0.48 wt%, originating from the 2-methylimidazole ligand of ZIF-67. Although present in small amounts, nitrogen doping is known to enhance the surface basicity and electron density of carbon materials, improving their affinity toward heavy metal ions (Gao et al., 2022).

The EDX elemental mapping (Figure 7, panels c–f) confirmed a uniform spatial distribution of all four elements across the particle surface with no visible phase segregation. The carbon map (yellow) covered the entire surface uniformly, confirming it as the dominant structural matrix. The oxygen map (red) showed strong signals concentrated on the surface and edges, indicating accessible oxygen-rich adsorption sites. The cobalt map (pink) revealed well-dispersed cobalt nanoparticles throughout the matrix without obvious agglomeration, which is favorable for maintaining a high density of active adsorption sites. The nitrogen map (blue) showed a low but evenly distributed signal consistent with its minor but meaningful incorporation into the carbon framework.

Overall, the FESEM-EDX results confirm the successful formation of a carbon-rich composite with well-dispersed cobalt nanoparticles and reactive oxygen-containing surface groups properties that are collectively expected to contribute to the effective adsorption of Cr(VI) and Pb(II) from aqueous solution.

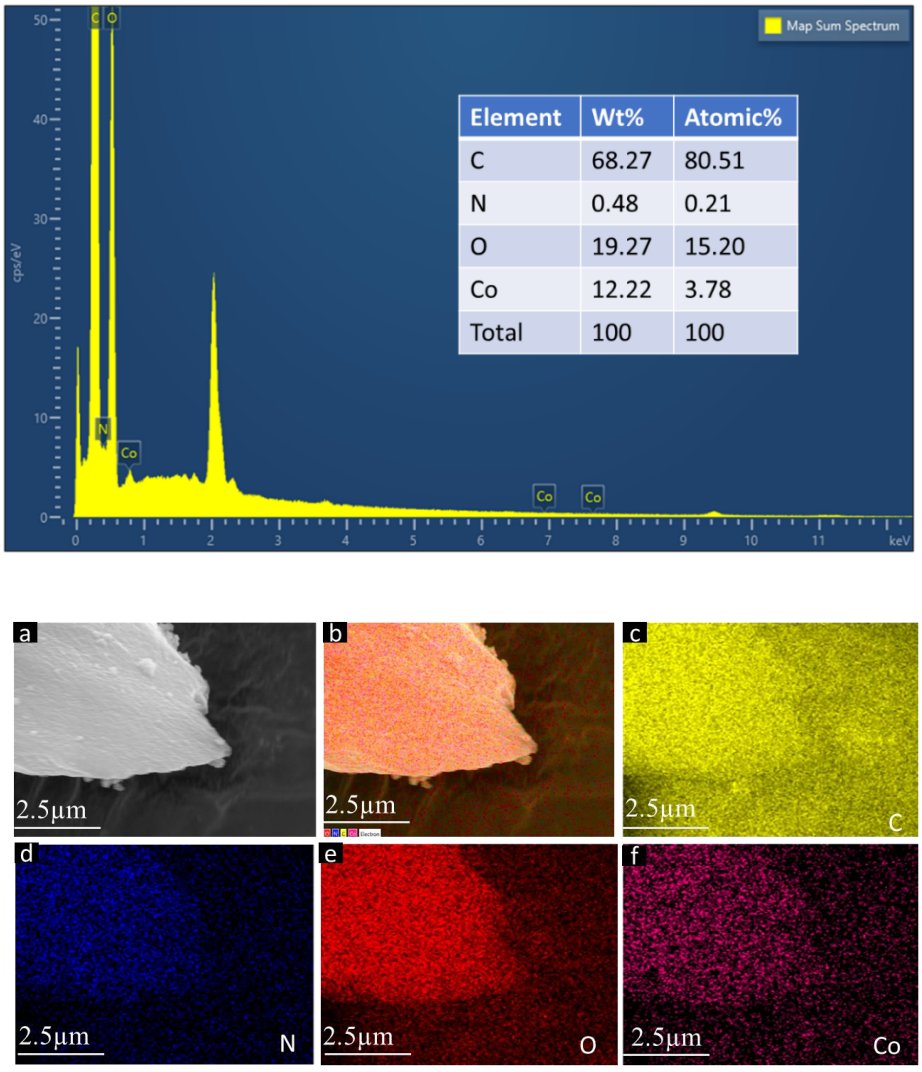

Figure 7: EDX and Elemental mapping of JSP-MOF900

4.4 X-Ray Diffraction Analysis

The X-ray diffraction (XRD) patterns for JSP-Pristine900 and JSP-MOF900 have been examined in Jeonbuk National University laboratory (XRD, Rigaku, Cu Kα (λ = 1.54056 Å, 40 kV, and 40

mA) to examine any differences in terms of their crystalline nature following carbonization at a temperature of 900 °C shown in figure 8. From the obtained data, it can be observed that there exists a large difference in the nature of these two samples.

Specifically, for JSP-Pristine900, one sees a diffraction pattern that consists of a broad peak for a diffraction angle, 2θ, of around 22–25°. The latter belongs to the (002) plane for an amorphous carbon form. Therefore, it can be said that the degree of graphitization is quite small in this case(Moseenkov et al., 2023). Furthermore, for $2\theta \approx 43–45°$, there exists a weak and broad pattern that belongs to the (100) plane. This suggests the existence of some graphitic domains(Manoj & Kunjomana, 2012).

The XRD pattern of JSP-MOF900 consists of a broad peak characteristic of carbon, as well as a few sharp peaks, suggesting that both amorphous carbon and crystalline phases are present in the material. The broad peak centered around $2\theta = 24°$ represents the carbon phase, identical to the one observed in the initial sample. Nevertheless, the presence of a few prominent sharp peaks centered at $2\theta = 31°$, 36°, 44°, and 59° shows that crystalline phases have been successfully synthesized by carbonization reactions(Li et al., 2021).

The identified sharp peaks correspond to cobalt-based materials, which are most likely Co_3O_4 and metallic Co^0 resulting from the decomposition of the ZIF-67 framework(Cai et al., 2025; Mamdouh et al., 2024). For example, the peak at $2\theta = 36°$ represents the (311) plane of Co_3O_4, whereas the peak near $2\theta = 44°$ is assigned to the (111) plane of metallic cobalt, with some contribution from the carbon (100) plane. Finally, the peaks around $2\theta = 59°$ may represent the (511) or (440) planes of Co_3O_4(Ravina et al., 2024).

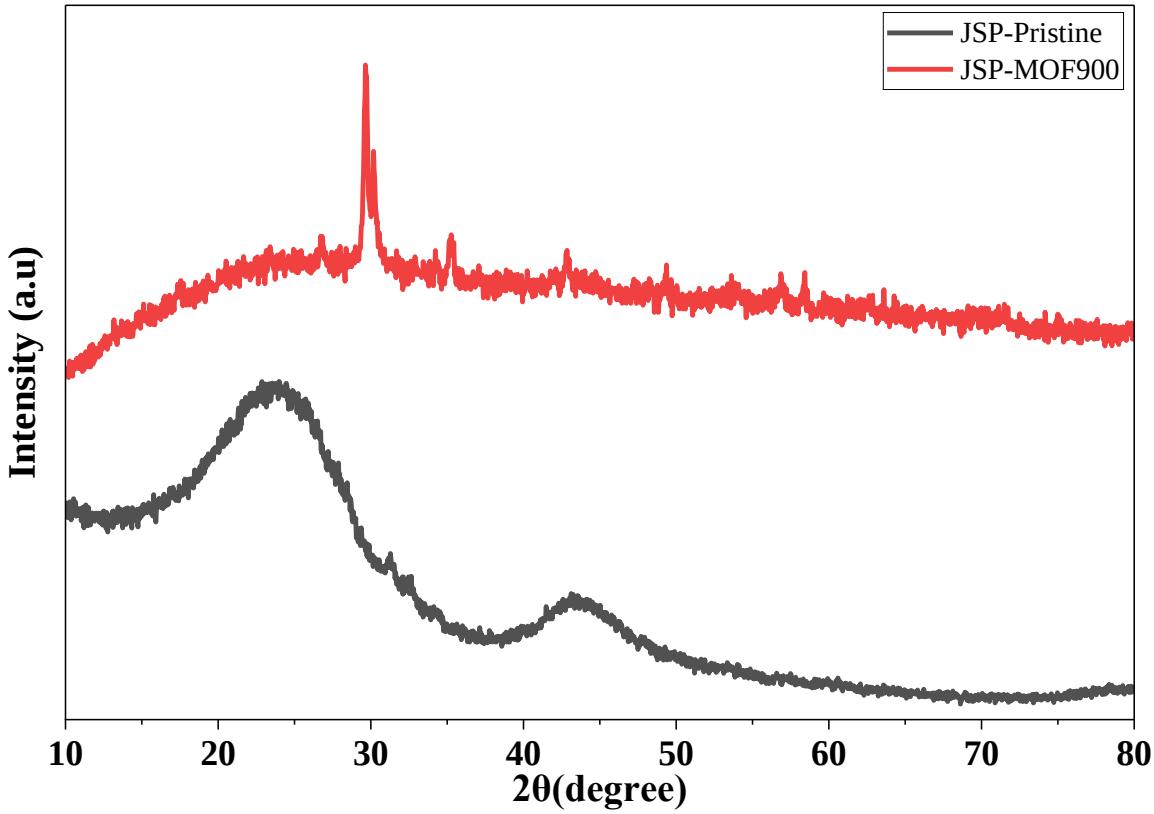

Figure 8: XRD plot of JSP-Pristine and JSP-MOF900

4.5 Adsorption Performance Analysis

4.5.1 UV-Vis Absorbance Study of Cr(VI) Removal Over Time

Adsorption efficiency of Cr(VI) through JSP-based materials was conducted via the technique of UV-visible spectroscopy by measuring the absorption spectrum of the complex between Cr(VI) ion and diphenylcarbazide at 540 nm (Emadi et al., 2022). The absorption of pristine JSP, JSP-MOF700, JSP-MOF800, and JSP-MOF900 were plotted. Because the absorption spectrum at 540 nm is directly related to the concentration of Cr(VI), decreasing in peak intensity means that the Cr(VI) ion is being removed.

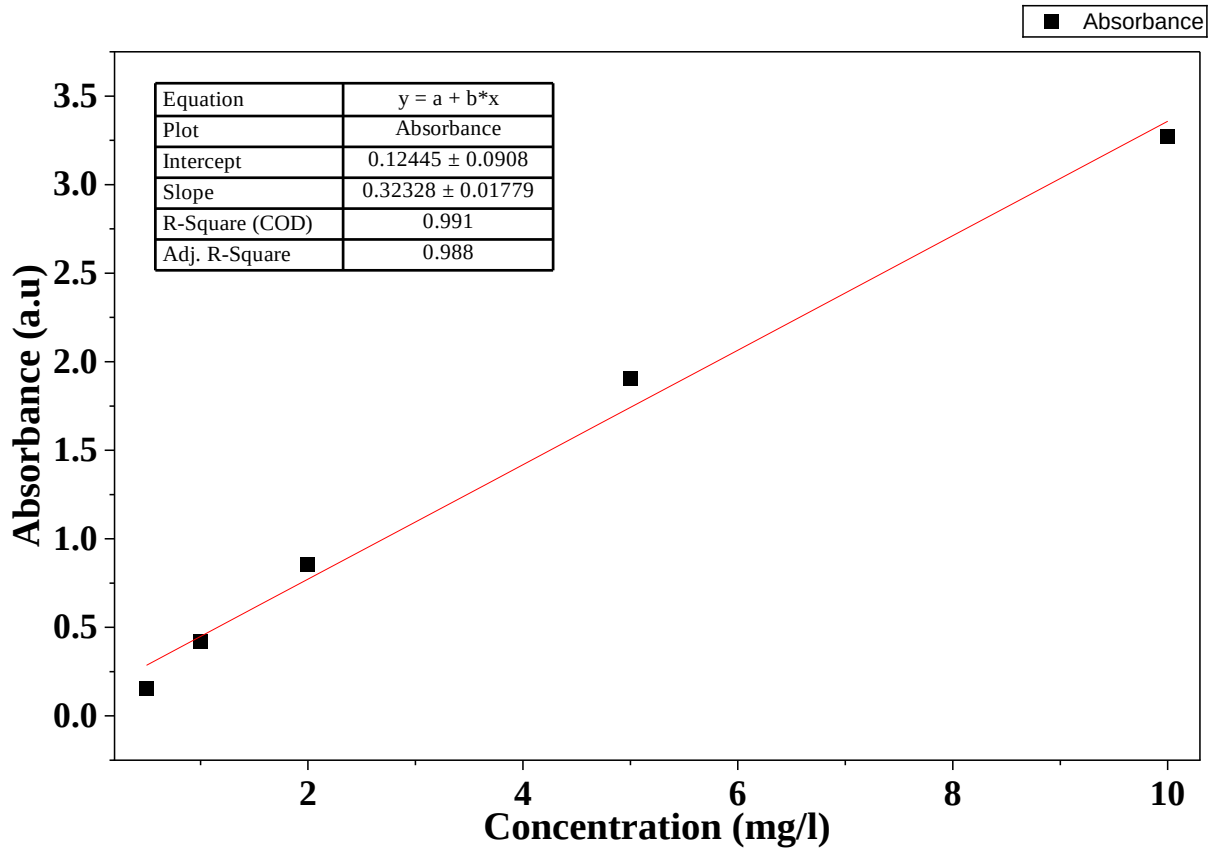

Figure 9: Calibration curve for Cr(VI) determination

Before analyzing the absorption samples, the calibration curve for determining the concentration of Cr(VI) in the solution through UV–Vis spectrophotometry (UV-2600i, Shimadzu, Nonlaboratory, Pulchowk Campus) was constructed as in figure 9. The standard Cr(VI) working solutions with various concentrations were prepared at pH 2 (Bhattarai et al., 2022; Emadi et al., 2022), and their absorbance at 540 nm was analyzed after mixing with 1,5-diphenylcarbazide reagent. It was revealed that there was a direct proportion between the increase in the concentration of Cr(VI) and the increase in absorbance, confirming the applicability of Beer-Lambert's law in this case(Dawra & Dabas, 2024).

Thus, there was a good correlation between the absorbance and concentration of Cr(VI), which is illustrated by the following regression equation:

$$y=0.12445+0.32328x, \ldots\ldots\ldots\ldots\ldots\ldots\ldots\ldots (7)$$

where y stands for absorbance, and x stands for the concentration of Cr(VI) in mg/L. R^2 is 0.991, meaning that there is an excellent linearity and reliability of the calibration curve, which makes it possible to use this regression equation for calculating the concentration of remaining Cr(VI) in adsorption tests based on their absorbance(Pehlivan & Cetin, 2009; Uysal & Ar, 2007).

Specifically, for each absorption sample, the absorbance was determined at 540 nm and substituted into the calibration equation to get the corresponding Cr(VI) concentration:

$$X = \frac{y-0.12445}{0.32328} \ldots\ldots\ldots\ldots\ldots\ldots\ldots\ldots\ldots\ldots\ldots\ldots (8)$$

Where X is the Cr(VI) concentration post-adsorption, and y is the absorbance measured. The obtained concentrations were used for further calculation of C/C_0 ratio, removal efficiency, and kinetics(Ahmad et al., 2016).

The calibration procedure was essential to make sure that UV-Vis absorbance readings are correctly transformed into concentrations of Cr(VI).

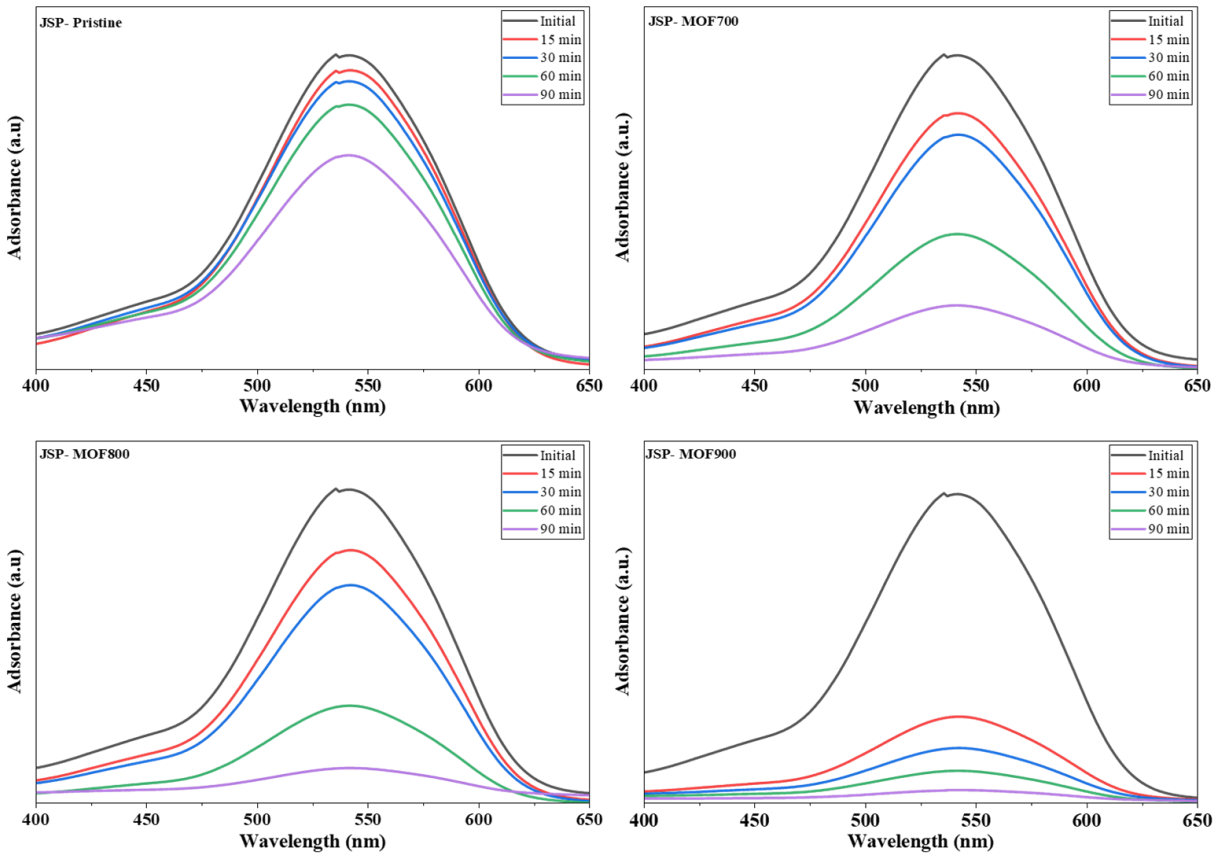

Figure 10: Time-dependent absorbance profiles of different samples

From the absorption spectra shown in Figure 10, it is apparent that the reduction in the absorbance spectra continues as the contact time increases. Therefore, it can be said that there is an ongoing process of removing Cr(VI) ions from the solution.

From among all the samples, JSP-MOF900 records the greatest drop in absorbance at all time points, implying that it has the best Cr(VI) removal efficacy. JSP-MOF800 is also observed to remove Cr(VI) ions effectively; however, its absorbance readings are higher compared to JSP-MOF900. The absorbance readings from JSP-MOF700 show moderate adsorption, whereas the JSP-Pristine sample has the least absorbance decline. Therefore, based on the experimental findings, the following ranking can be suggested for the performance of the samples under investigation:

JSP-MOF900 > JSP-MOF800 > JSP-MOF700 > JSP-Pristine

The enhanced performance of JSP-MOF900 might be the carbonization temperature influencing adsorption efficacy. Specifically, when the material is subjected to high temperatures of 900°C, the carbon structure is graphitized and electrical conductivity is improved, leading to efficient electron transfer reactions. Also, the degradation of ZIF-67 structure results in the dispersion of Co-based nanoparticles, which serve as active centers and increase the adsorbate–adsorbent interaction. Moreover, these active centers might be able to reduce Cr(VI) ions into the less toxic Cr(III) form, thus promoting adsorption-reduction synergy.

On the other hand, JSP-MOF700 can be affected by incomplete carbonization, leading to poor pore development and fewer active adsorption sites. JSP-MOF800, despite having an advanced porous structure and considerable adsorption efficiency, might have lower catalytic activity than JSP-MOF900. JSP-Pristine is found to be least efficient because of minimal surface area without any engineering pores and active sites.

Kinetic study is conducted via pseudo-first-order analysis based on plots of $-\ln(C/C_0)$ against contact time. Linear trends generated by such plots reveal that adsorption is in accordance with pseudo-first-order kinetics, where the rate of adsorption is proportional to the concentration of Cr(VI) ions. The gradient of each graph denotes the rate constant (k), which indicates the rate of adsorption.

Based on the kinetic data, it is evident that JSP-MOF900 has the highest slope value, suggesting the fastest adsorption rate among all samples. In comparison, JSP-MOF800 has the second fastest rate, followed by JSP-MOF700, whereas JSP-Pristine has the slowest rate. These results are in agreement with the findings of UV-Vis absorbance analysis. Thus, JSP-MOF900 proves to be the best adsorbent material for Cr(VI) ions.

Overall, the UV-Vis spectroscopic and kinetic measurements indicate that JSP-MOF900 has the best efficiency for removal and fastest adsorption kinetics. In addition, higher carbonization temperatures contribute to improved structure as well as catalytic activity, which result in better performance for the removal of Cr(VI). For JSP-MOF900, Cr(VI) adsorption consists of fast initial

adsorption kinetics followed by slow attainment of equilibrium. This is due to the occurrence of surface adsorption and reduction mechanisms.

4.5.2 Comparative Adsorption Capacity

Figure 11 represents a comparative bar chart of the adsorption capacity of JSP-Pristine, JSP-MOF700, JSP-MOF800, and JSP-MOF900 across different experimental conditions. Several important trends emerge from this comparison.

First, JSP-Pristine consistently exhibited the lowest adsorption capacity across all tested conditions, confirming that the raw Jacaranda seed pod biomass without MOF growth and carbonization has limited capability for Cr(VI) removal. This is expected given its relatively low surface area and the absence of the cobalt nanoparticles and nitrogen-doped carbon framework that characterize the MOF-derived composites.

Second, all three carbonized MOF composites JSP-MOF700, JSP-MOF800, and JSP-MOF900 showed markedly higher adsorption capacities than JSP-Pristine, clearly demonstrating the enhancement achieved through ZIF-67 growth and subsequent carbonization. This improvement is attributed to the synergistic contribution of the porous carbon matrix, retained oxygen surface groups, and dispersed cobalt nanoparticles all confirmed by EDX analysis which collectively provide a rich and accessible network of adsorption sites.

Third, and most significantly, JSP-MOF-900 demonstrated the highest adsorption capacity among all materials across the majority of tested conditions, establishing it as the optimal composite in this series. The superior performance of JSP-MOF900 over JSP-MOF800 and JSP-MOF700 reflects the benefit of higher carbonization temperature in developing a more graphitized, porous carbon structure with greater surface area.

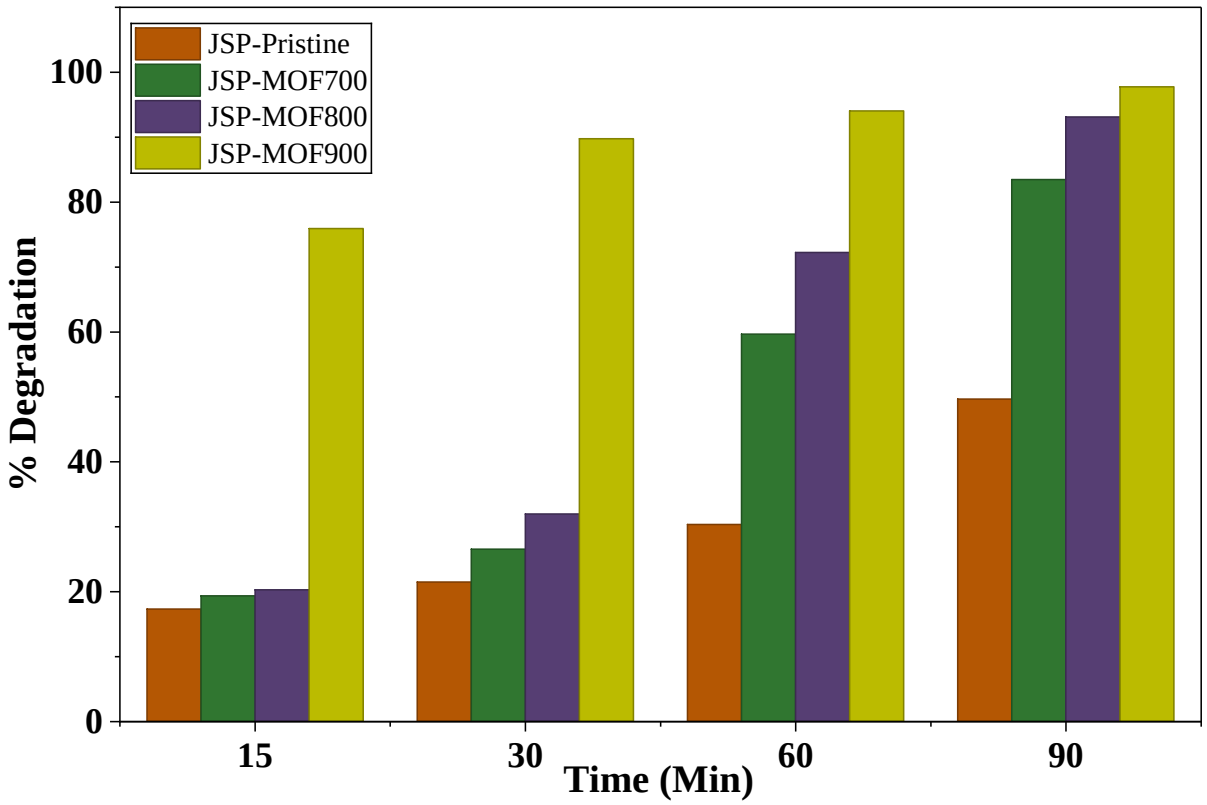

Figure 11: Comparative bar chart of adsorption capacity

The Graphs C/C_0 versus contact time in figure 12 represent the kinetics of removal of Cr(VI) ions from an aqueous solution using pristine carbon composites and MOF-derived carbon composites. It can be seen that the removal rate increases continuously with the contact time; however, there is a sudden decrease in the ratio. This shows that removal of Cr(VI) ions occurs quickly at first, and then slowly approaches the equilibrium level. The best performance is exhibited by the composite prepared at the highest temperature (JSP-MOF900), which removes almost all Cr(VI) ions in about 90 minutes. The MOF composite prepared at the lower temperature (JSP-MOF800) shows good removal but slower kinetics compared to the JSP-MOF900 sample. On the other hand, JSP-MOF700 removes less Cr(VI) ions with even slower kinetics. In addition, JSP-Pristine shows the poorest removal because it does not have any developed pores and active sites for adsorption reactions. This is due to higher graphitization, porosity, and availability of cobalt nanoparticles in JSP-MOF900.

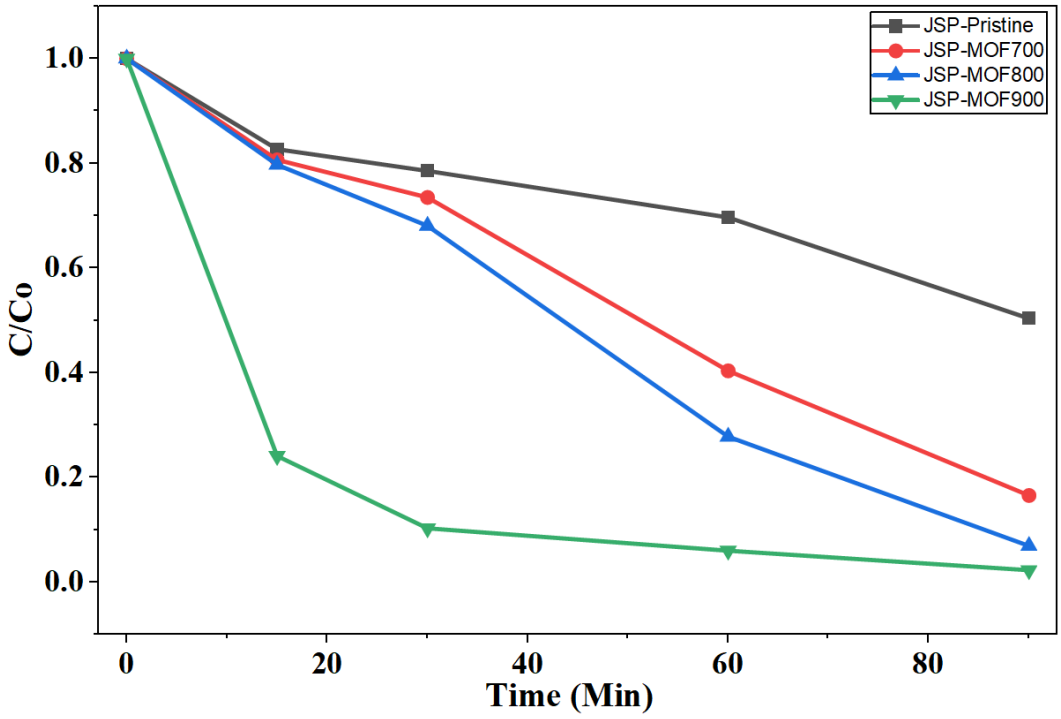

Figure 12: C/C_0 versus contact time graph

Kinetic profile analysis $-\ln(C/C_0)$ versus contact time in figure 13 gives an idea about the mechanism of Cr(VI) adsorption by pristine and carbon composites derived from metal-organic frameworks (MOFs). The obtained linear plots for all samples signify that the adsorption process approximately obeys the pseudo-first order reaction kinetics. Among the various adsorbents, the slope of the curve for JSP-MOF900 is high, indicating the maximum value of the rate constant and maximum rate of removal. The high efficiency of JSP-MOF900 is due to the formation of active sites as a result of better graphitization and dispersion of Co nanoparticles at 900°C temperature; apart from these active sites, reduction to Cr(III) also takes place. Slightly lower kinetics of JSP-MOF800 indicate that even though it had a well-developed porous system, it had relatively poor catalytic ability. The performance of JSP-MOF700 was moderate because of the insufficient degree of carbonization; similarly, JSP-Pristine showed very low adsorption ability because there was no porosity present in it.

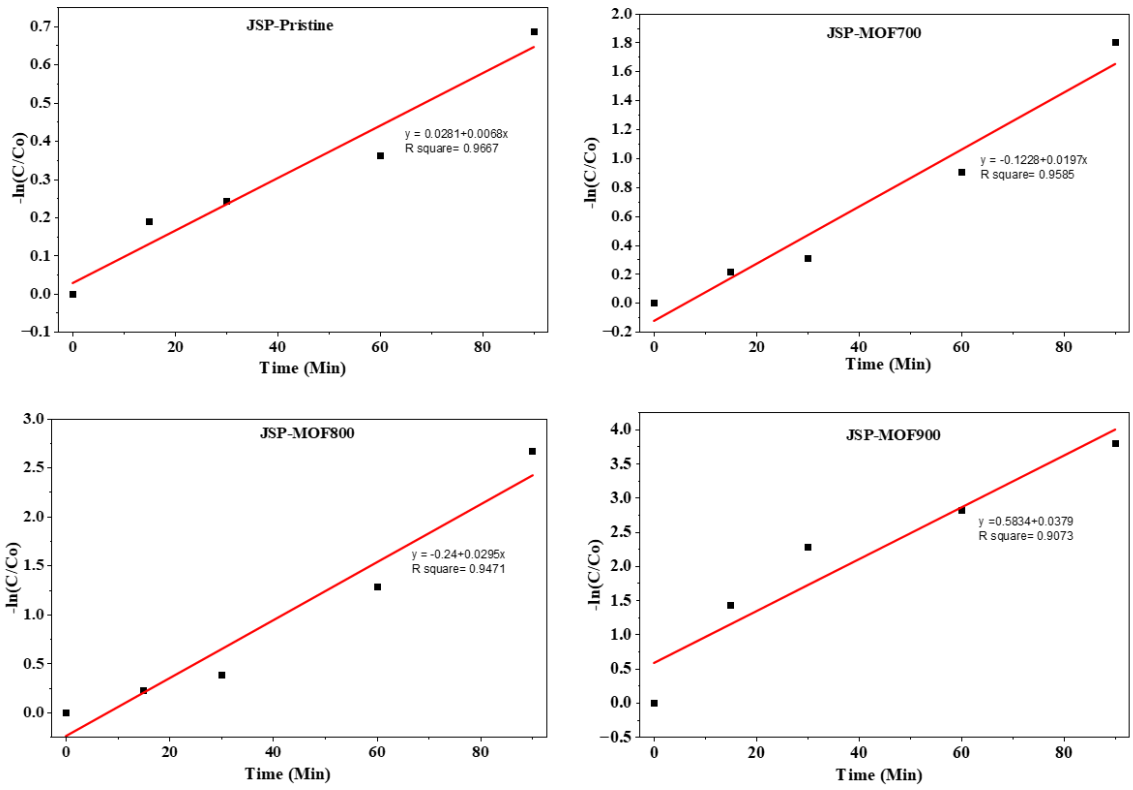

Figure 13: Pseudo First Order Analysis Graph

Table 3: Pseudo First Order Parameters (K and R^2) for Cr(VI) Adsorption

Sample	**R^2 Value**	**Slope K (Rate Constant)**
JSP-Pristine	0.9667	0.0068
JSP-MOF700	0.9585	0.0197
JSP-MOF800	0.9471	0.0295
JSP-MOF900	0.9073	0.0379

To test the applicability of the pseudo-first order kinetic equation, a graph of $-\ln(C/C_0)$ against time resulted in straight-line plots for all adsorbents tested. The slope of these lines is the value of the rate constant (k) and denotes the rate of Cr(VI) adsorption as in figure 14. Among all adsorbents tested, JSP-MOF900 possessed the largest slope value as shown in table 2 and is therefore associated with the highest rate of adsorption kinetics, followed by JSP-MOF800, JSP-MOF700, and finally JSP-Pristine. In addition to the rate constant value, the quality of data fitting with the kinetic model was determined through the coefficient of determination (R^2). The obtained values of R^2 for all adsorbents were close to unity ($R^2 > 0.90$), signifying an excellent fit of data with the pseudo-first-order model. The closer the value of R^2 to 1.0, the more the experimental data agrees with the model predictions, and therefore, the concentration-dependent nature of kinetics can be inferred from this information.

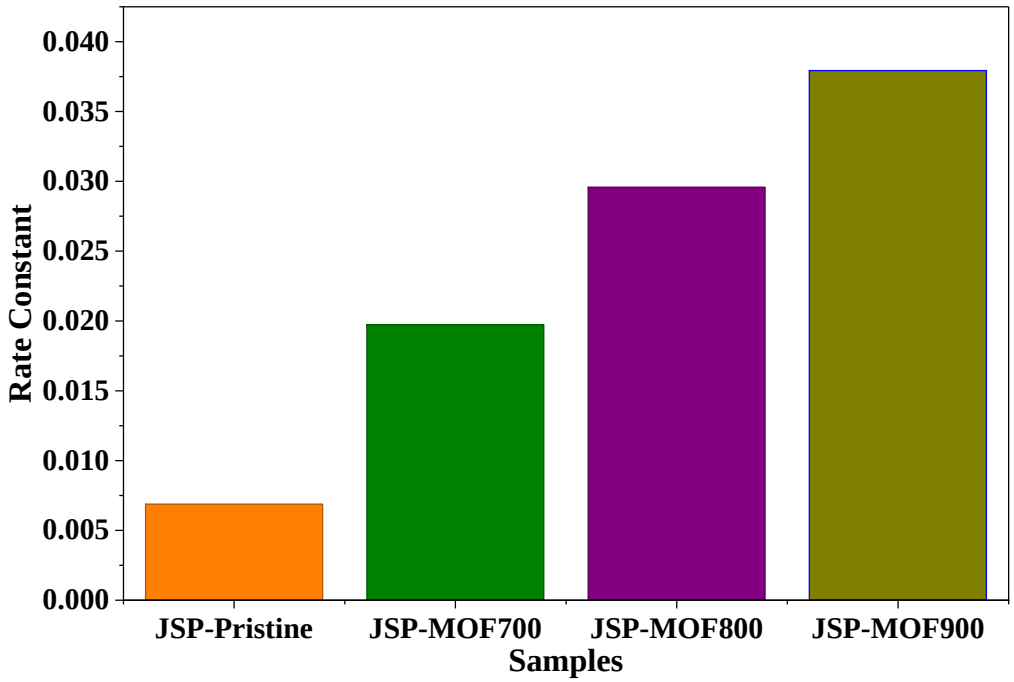

Figure 14: Rate Constant of different sample

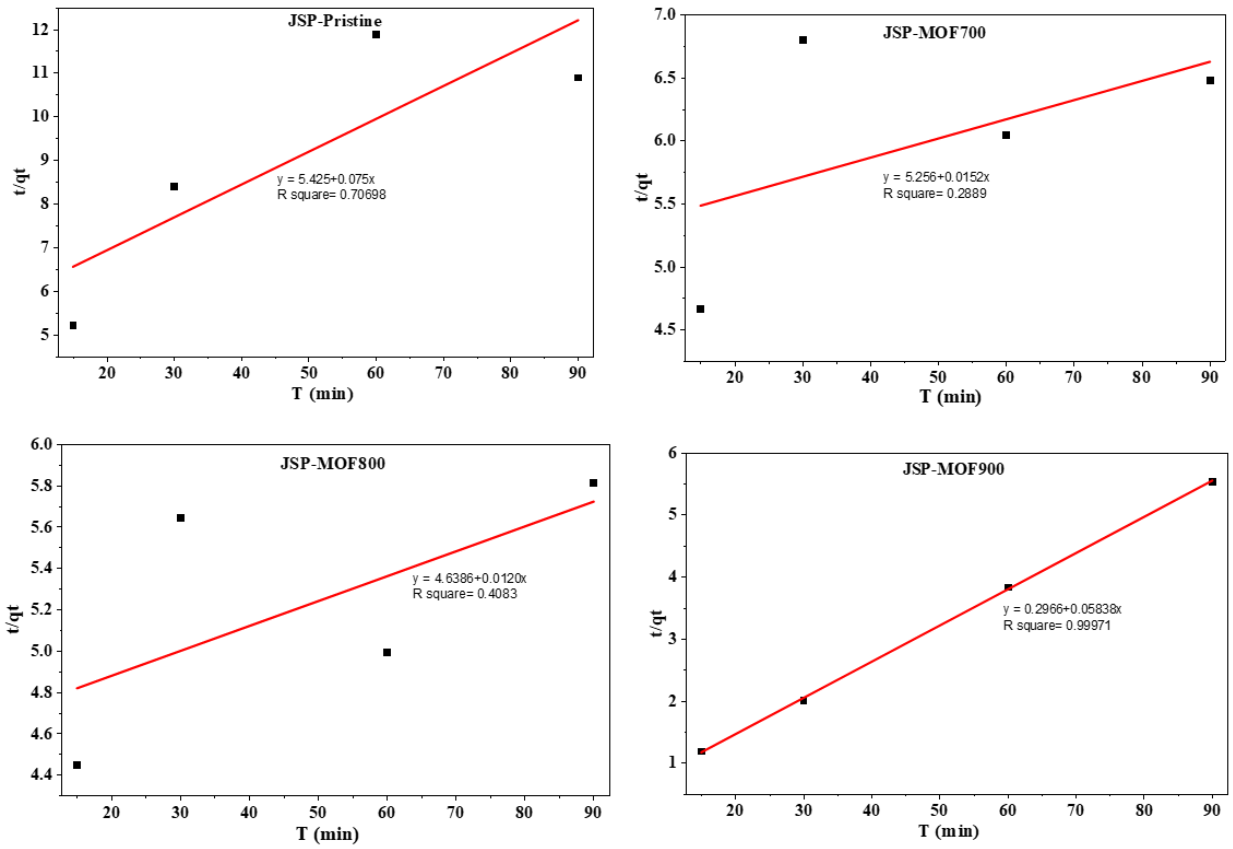

Figure 15: Pseudo Second Order Analysis Graph

Further analysis was conducted using the pseudo-second-order (PSO) model where a graph of t/q_t against time, t, was plotted for each adsorbent. Figure 15 reveals that although adsorbents JSP-Pristine, JSP-MOF700, and JSP-MOF800 show relatively low R^2 values when fitted using the PSO model, JSP-MOF900 gives an unusually high value of R^2 indicating a better fit, hence its adsorption process follows PSO best.

It is clear from the above analysis that chemisorption is the main rate- controlling step in the adsorption process of adsorbent JSP-MOF900. This process involves the formation of strong chemical bonds possibly due to electrostatic attraction, surface complexation, and ion exchange between Cr(VI) anions such as $HCrO_4^-$ and $Cr_2O_7^{2-}$ and active sites on the JSP-MOF900 suggests that there must be some structural and composition changes in the MOF, hence increased

availability of active sites on the surface of JSP-MOF900 compared to JSP-MOF700 and JSP-MOF800.

Table 4: Summary of Kinetics fitting model

Sample	**PFO R^2**	**PFO Model Fit**	**PSO R^2**	**PSO Model Fit**
JSP-Pristine	High	Satisfies	Moderate	Does not satisfy
JSP-MOF700	High	Satisfies	Low	Does not satisfy
JSP-MOF800	High	Satisfies	Low	Does not satisfy
JSP-MOF900	High	Satisfies	High (Highest)	Strongly Satisfy

So, pseudo-first-order kinetic studies which were carried out on the adsorption of Cr(VI) onto JSP-Pristine, JSP-MOF700, JSP-MOF800, and JSP-MOF900 to confirm that all four adsorbents have pseudo-first-order kinetics. This indicates that processes like physisorption and diffusion significantly contribute to the mechanism involved in adsorption. Also, the adsorption of Cr(VI) ions onto JSP-MOF900,prepared by carbonization at the highest temperature(900 °C), shows the highest correlation with the pseudo-second-order model compared to other adsorbents. This shows that the mechanism of adsorption in such an adsorbent is mainly chemisorption, and this may be due to the increased reactivity and concentration of functional sites on the surface of the adsorbent due to thermal conversion at high temperatures.

CHAPTER 5: CONCLUSIONS AND RECOMMENDATION

Conclusion

This study successfully developed carbon-based MOF composites from Jacaranda seed pod biomass and tested their ability to remove chromium from water. Among all composites prepared, JSP-MOF900 performed best, removing approximately 97% of Cr(VI) from aqueous solution.

The removal worked through two key steps. First, at acidic pH 2, the positively charged surface of the adsorbent attracted Cr(VI) ions quickly followed pseudo first-order kinetics. Second, cobalt species within the composite triggered a chemical reaction that converted the more harmful Cr(VI) into the less toxic Cr(III), which then either stuck to the surface or settled out of solution consistent with pseudo second-order kinetics.

Overall, these results confirm that Jacaranda seed pod waste can be turned into an effective, low-cost material for cleaning up chromium-contaminated wastewater.

Recommendation

Based on these findings, the following is recommended:

- Future studies should test JSP-MOF900 on real industrial wastewater samples to confirm performance under practical conditions.
- Further research should explore regeneration and reusability of the composite to assess its long-term cost-effectiveness.
- Scaling up the synthesis process should be investigated to support larger-scale water treatment applications.
- Testing the material against other heavy metal contaminants would help broaden its potential environmental applications.

References

Ahalya, N., Ramachandra, T., & Kanamadi, R. (2003). Biosorption of heavy metals. Res. J. Chem. Environ, 7(4), 71–79.

Ahmad, W., Bashammakh, A., Al-Sibaai, A., Alwael, H., & El-Shahawi, M. (2016). Trace determination of Cr (III) and Cr (VI) species in water samples via dispersive liquid-liquid microextraction and microvolume UV–Vis spectrometry. Thermodynamics, speciation study. Journal of Molecular Liquids, 224, 1242–1248.

Ahuja, S. (2015). Overview of Global Water Challenges and Solutions. In Water Challenges and Solutions on a Global Scale (Vol. 1206, pp. 1–25). American Chemical Society. https://doi.org/doi:10.1021/bk-2015-1206.ch001

10.1021/bk-2015-1206.ch001

Akhtar, M. S., Ali, S., & Zaman, W. (2024). Innovative adsorbents for pollutant removal: exploring the latest research and applications. Molecules, 29(18), 4317.

Ali, A., Alharthi, S., Al-Shaalan, N. H., Naz, A., & Fan, H.-J. S. (2023). Efficient removal of hexavalent chromium (Cr (VI)) from wastewater using amide-modified biochar. Molecules, 28(13), 5146.

Amin, M., Shah, H. H., Usman, M., & Iqbal, M. A. (2025). The environmental impacts via life cycle assessment of activated carbon produced by Fiddlewood and Jacaranda biomass. Clean Technologies and Environmental Policy, 27(7), 3129–3144.

Aragaw, T. A., & Bogale, F. M. (2021). Biomass-based adsorbents for removal of dyes from wastewater: a review. Frontiers in Environmental Science, 9, 764958.

Ayach, J., El Malti, W., Duma, L., Lalevée, J., Al Ajami, M., Hamad, H., & Hijazi, A. (2024). Comparing conventional and advanced approaches for heavy metal removal in wastewater treatment: an in-depth review emphasizing filter-based strategies. Polymers, 16(14), 1959.

Azeez, S., & Shenbagaraman, R. (2025). Fourier transform infrared spectroscopy in characterization of bionanocomposites. In Characterization Techniques in Bionanocomposites (pp. 209–227). Elsevier.

Azimi, A., Azari, A., Rezakazemi, M., & Ansarpour, M. (2017). Removal of heavy metals from industrial wastewaters: a review. ChemBioEng Reviews, 4(1), 37–59.

Azmi, L. S., Jabit, N. A., Ismail, S., Ku Ishak, K. E. H., & Abdullah, T. K. (2025). Membrane filtration technologies for sustainable industrial wastewater treatment: a review of heavy metal removal. Desalination and Water Treatment, 323, 101321. https://doi.org/https://doi.org/10.1016/j.dwt.2025.101321

Beţianu, C., Cozma, P., & Gavrilescu, M. (2024). Human health hazards and risks generated by the bioaccumulation of lead from the environment in the food chain. In Lead Toxicity Mitigation: Sustainable Nexus Approaches (pp. 73–123). Springer.

Bhattarai, K. P., Pant, B. D., Rai, R., Aryal, R. L., Paudyal, H., Gautam, S. K., Ghimire, K. N., Pokhrel, M. R., & Poudel, B. R. (2022). Efficient sequestration of Cr (VI) from aqueous solution using biosorbent derived from Arundo donax stem. Journal of Chemistry, 2022(1), 9926391.

Briffa, J., Sinagra, E., & Blundell, R. (2020). Heavy metal pollution in the environment and their toxicological effects on humans. Heliyon, 6(9), e04691. https://doi.org/https://doi.org/10.1016/j.heliyon.2020.e04691

Cai, Y., Liu, X., Yang, W., Peng, H., Meng, L., & Zhao, S. (2025). Preparation of cobalt based organic metal framework ZIF-67 catalyst for activating PMS and its catalytic system for rapid degradation of various high concentration dyes.

Castro, K., & Abejón, R. (2024). Removal of heavy metals from wastewaters and other aqueous streams by pressure-driven membrane technologies: An outlook on reverse osmosis, nanofiltration, ultrafiltration and microfiltration potential from a bibliometric analysis. Membranes, 14(8), 180.

Chai, L., Li, R., Sun, Y., Zhou, K., & Pan, J. (2025). MOF-derived carbon-based materials for energy-related applications. Advanced materials, 37(8), 2413658.

Chakraborty, R., Asthana, A., Singh, A. K., Jain, B., & Susan, A. B. H. (2022). Adsorption of heavy metal ions by various low-cost adsorbents: a review. International Journal of Environmental Analytical Chemistry, 102(2), 342–379.

Chandran, D. G., Muruganandam, L., & Biswas, R. (2023). A review on adsorption of heavy metals from wastewater using carbon nanotube and graphene-based nanomaterials. Environmental Science and Pollution Research, 30(51), 110010–110046.

Chongdar, S., Bhattacharjee, S., Bhanja, P., & Bhaumik, A. (2022). Porous organic–inorganic hybrid materials for catalysis, energy and environmental applications. Chemical Communications, 58(21), 3429–3460.

Cossu, L. O., De Aquino, S. F., Mota Filho, C. R., Smith, C. J., & Vignola, M. (2024). Review on Pesticide Contamination and Drinking Water Treatment in Brazil: The Need for Improved Treatment Methods. ACS ES&T Water, 4(9), 3629–3644. https://doi.org/10.1021/acsestwater.4c00063

Darban, Z., Shahabuddin, S., Gaur, R., Ahmad, I., & Sridewi, N. (2022). Hydrogel-based adsorbent material for the effective removal of heavy metals from wastewater: A comprehensive review. Gels, 8(5), 263.

Dawra, N., & Dabas, N. (2024). Advances in spectrophotometric determination of Chromium (III) and Chromium (VI) in water: a review. International Journal of Environmental Analytical Chemistry, 104(13), 2994–3015.

Ding, J., Tang, Y., Zheng, S., Zhang, S., Xue, H., Kong, Q., & Pang, H. (2022). The synthesis of MOF derived carbon and its application in water treatment. Nano Research, 15(8), 6793–6818.

El-Azazy, M., El-Shafie, A. S., & Al-Saad, K. (2022). Application of infrared spectroscopy in the characterization of lignocellulosic biomasses utilized in wastewater treatment. In Infrared spectroscopy-perspectives and applications. IntechOpen.

Emadi, Z., Sadeghi, M., Forouzandeh, S., Sadeghi, R., Sadeghi, R., & Mohammadi-Moghadam, F. (2022). Simultaneous decolorization/degradation of AB-113 and chromium (VI) removal by a salt-tolerant Klebsiella sp. AB-PR and detoxification of biotransformed-metabolites. International journal of Environmental Science and Technology, 19(3), 2007–2024.

Ethaib, S., Al-Qutaifia, S., Al-Ansari, N., & Zubaidi, S. L. (2022). Function of nanomaterials in removing heavy metals for water and wastewater remediation: A review. Environments, 9(10), 123.

Ganjoo, R., Sharma, S., Kumar, A., & Daouda, M. (2023). Activated carbon: fundamentals, classification, and properties.

Gao, K., Li, J., Chen, M., Jin, Y., Ma, Y., Ou, G., & Wei, Z. (2021). ZIF-67 derived magnetic nanoporous carbon coated by poly (m-phenylenediamine) for hexavalent chromium removal. Separation and Purification Technology, 277, 119436.

Ghimire, S., Pokhrel, N., Pant, S., Gyawali, T., Koirala, A., Mainali, B., Angove, M. J., & Paudel, S. R. (2022). Assessment of technologies for water quality control of the Bagmati River in Kathmandu valley, Nepal. Groundwater for Sustainable Development, 18, 100770. https://doi.org/https://doi.org/10.1016/j.gsd.2022.100770

Hamadneh, I., Jukhan, M. A., Damer, K., Alkhaza'leh, H., Hammad, H., Qanadilo, S., & Al-Dujaili, A. H. (2026). Preparation and Adsorption Properties of Biochar Derived from Biomass of Jacaranda mimosifolia Fruit Pod for the Removal of Cr (VI) Ion from Aqueous Solution. Water, Air, & Soil Pollution, 237(2), 70.

Hamda, A. S., Areti, H. A., Gudeta, R. L., Abo, L. D., & Jayakumar, M. (2025). Carbon-based nanomaterials for water treatment: A comprehensive review of recent advances and mechanisms. Chemical Engineering Journal Advances, 23, 100834. https://doi.org/https://doi.org/10.1016/j.ceja.2025.100834

Hanikel, N., Prévot, M. S., & Yaghi, O. M. (2020). MOF water harvesters. Nature nanotechnology, 15(5), 348–355.

He, M., Xu, Z., Hou, D., Gao, B., Cao, X., Ok, Y. S., Rinklebe, J., Bolan, N. S., & Tsang, D. C. (2022). Waste-derived biochar for water pollution control and sustainable development. Nature Reviews Earth & Environment, 3(7), 444–460.

Hussain, M., Ali, V., Pourebrahimi, S., Ahmadi, S., & Ghosh, S. (2023). Chemical methods of heavy metal management: Coagulation, flocculation, and floatation. In Heavy Metals in the Environment: Management Strategies for Global Pollution (pp. 297–312). ACS Publications.

Jadhav, H. S., Bandal, H. A., Ramakrishna, S., & Kim, H. (2022). Critical review, recent updates on zeolitic imidazolate framework-67 (ZIF-67) and its derivatives for electrochemical water splitting. Advanced materials, 34(11), 2107072.

Jagaba, A. H., Lawal, I. M., Birniwa, A. H., Affam, A. C., Usman, A. K., Soja, U. B., Saleh, D., Hussaini, A., Noor, A., & Yaro, N. S. A. (2024). Sources of water contamination by heavy

metals. In Membrane technologies for heavy metal removal from water (pp. 3–27). CRC Press.

Jiang, J., Shi, Y., Wu, M., Rezakazemi, M., Aminabhavi, T. M., Huang, R., Jia, C., & Ge, S. (2024). Biomass-MOF composites in wastewater treatment, air purification, and electromagnetic radiation adsorption–A review. Chemical Engineering Journal, 494, 152932.

Karki, A. (2025). Preparation of Activated Carbon from Jacaranda Seed Pods as Anode Material in Supercapacitors Pulchowk Campus].

Khine, Y. Y., Wen, X., Jin, X., Foller, T., & Joshi, R. (2022). Functional groups in graphene oxide. Physical Chemistry Chemical Physics, 24(43), 26337–26355.

Kikuchi, T., & Tanaka, S. (2012). Biological removal and recovery of toxic heavy metals in water environment. Critical Reviews in Environmental Science and Technology, 42(10), 1007–1057.

Kumar, P., Bansal, V., Kim, K.-H., & Kwon, E. E. (2018). Metal-organic frameworks (MOFs) as futuristic options for wastewater treatment. Journal of Industrial and Engineering Chemistry, 62, 130–145.

Kundu, C., Biswas, S., Thomas, B. S., Appadoo, D., Duan, A., & Bhattacharya, S. (2023). Evolution of functional group of lignocellulosic biomass and its delignified form during thermal conversion using synchrotron-based THz and laboratory-based in-situ DRIFT spectroscopy. Fuel, 348, 128579.

Ley, C. J., Proctor, C. R., Jordan, K., Ra, K., Noh, Y., Odimayomi, T., Julien, R., Kropp, I., Mitchell, J., Nejadhashemi, A. P., Whelton, A. J., & Aw, T. G. (2020). Impacts of Municipal Water–Rainwater Source Transitions on Microbial and Chemical Water Quality Dynamics at the Tap. Environmental Science & Technology, 54(18), 11453–11463. https://doi.org/10.1021/acs.est.0c03641

Li, K., Liu, Q., Cheng, H., Hu, M., & Zhang, S. (2021). Classification and carbon structural transformation from anthracite to natural coaly graphite by XRD, Raman spectroscopy, and HRTEM. Spectrochimica Acta Part A: Molecular and Biomolecular Spectroscopy, 249, 119286.

Li, R., Wang, X., Lin, C., Zhang, X., & Yuan, Z. (2025). The synergistic effect of MOF and biomass achieving dual breakthroughs in material structure and performance. Journal of Materials Chemistry A, 13(10), 6866–6894.

Li, X., Zheng, S., Jin, L., Li, Y., Geng, P., Xue, H., Pang, H., & Xu, Q. (2018). Metal-organic framework-derived carbons for battery applications. Advanced Energy Materials, 8(23), 1800716.

Liu, W., Liu, L., Yang, Z., Xu, J., Hou, Y., & Ji, G. (2018). A versatile route toward the electromagnetic functionalization of metal–organic framework-derived three-dimensional nanoporous carbon composites. ACS applied materials & interfaces, 10(10), 8965–8975.

Mamdouh, N., Farghali, A. A., El Rouby, W. M., & Abdelwahab, A. (2024). Effect of ZIF-67-derived Co3O4 on the activity of CNTs/NiCo2O4 nanocomposite for methanol oxidation reaction. International Journal of Hydrogen Energy, 93, 878–887.

Manoj, B., & Kunjomana, A. (2012). Study of stacking structure of amorphous carbon by X-ray diffraction technique. International Journal of Electrochemical Science, 7(4), 3127–3134.

McDowell, R. W., Luo, D., Pletnyakov, P., Upsdell, M., & Dodds, W. K. (2025). Anthropogenic nutrient inputs cause excessive algal growth for nearly half the world's population. Nature Communications, 16(1), 1830. https://doi.org/10.1038/s41467-025-57054-8

Md Salim, R., Asik, J., & Sarjadi, M. S. (2021). Chemical functional groups of extractives, cellulose and lignin extracted from native Leucaena leucocephala bark. Wood Science and Technology, 55(2), 295–313.

Mishra, S., Bharagava, R. N., More, N., Yadav, A., Zainith, S., Mani, S., & Chowdhary, P. (2018). Heavy metal contamination: an alarming threat to environment and human health. In Environmental biotechnology: For sustainable future (pp. 103–125). Springer.

Mohamed, M. A., Jaafar, J., Ismail, A., Othman, M., & Rahman, M. (2017). Fourier transform infrared (FTIR) spectroscopy. In Membrane characterization (pp. 3–29). Elsevier.

Moseenkov, S., Kuznetsov, V., Zolotarev, N., Kolesov, B., Prosvirin, I., Ishchenko, A., & Zavorin, A. (2023). Investigation of amorphous carbon in nanostructured carbon materials (a comparative study by TEM, XPS, Raman spectroscopy and XRD). Materials, 16(3), 1112.

Motshekga, S. C., Oyewo, O. A., & Makgato, S. S. (2024). Recent and prospects of synthesis and application of metal-organic frameworks (MOFs) in water treatment: a review. Journal of Inorganic and Organometallic Polymers and Materials, 34(9), 3907–3930.

Mukhiya, T., Muthurasu, A., Tiwari, A. P., Chhetri, K., Chae, S.-H., Kim, H., Dahal, B., Lee, B. M., & Kim, H. Y. (2021). Integrating the essence of a metal–organic framework with electrospinning: a new approach for making a metal nanoparticle confined N-doped carbon nanotubes/porous carbon nanofibrous membrane for energy storage and conversion. ACS applied materials & interfaces, 13(20), 23732–23742.

Munir, N., Jahangeer, M., Bouyahya, A., El Omari, N., Ghchime, R., Balahbib, A., Aboulaghras, S., Mahmood, Z., Akram, M., & Ali Shah, S. M. (2021). Heavy metal contamination of natural foods is a serious health issue: A review. Sustainability, 14(1), 161.

Mustapha, L. S., Obayomi, O. V., Yahya, M. D., Lau, S. Y., & Obayomi, K. S. (2024). Exploring the synergistic effects of calcium chloride modification on stem bark eucalyptus biochar for Cr (VI) and Pb (II) ions removal: Kinetics, isotherm, thermodynamic and optimization studies. Bioresource Technology Reports, 25, 101699.

Nascimento, J. M. d., Otaviano, J. J. S., Sousa, H. S. d., & Oliveira, J. D. d. (2023). Biological method of heavy metal management: Biosorption and bioaccumulation. Heavy Metals in the Environment: Management Strategies for Global Pollution, 315–360.

Nnaji, N. D., Onyeaka, H., Miri, T., & Ugwa, C. (2023). Bioaccumulation for heavy metal removal: a review. SN Applied Sciences, 5(5), 125.

Oladimeji, T. E., Oyedemi, M., Emetere, M. E., Agboola, O., Adeoye, J. B., & Odunlami, O. A. (2024). Review on the impact of heavy metals from industrial wastewater effluent and removal technologies. Heliyon, 10(23), e40370. https://doi.org/https://doi.org/10.1016/j.heliyon.2024.e40370

Omer, A. M., Abd El-Monaem, E. M., Abd El-Latif, M. M., El-Subruiti, G. M., & Eltaweil, A. S. (2021). Facile fabrication of novel magnetic ZIF-67 MOF@ aminated chitosan composite beads for the adsorptive removal of Cr (VI) from aqueous solutions. Carbohydrate Polymers, 265, 118084.

Patel, V. H., Gani, A., & Paul, A. (2025). Single-Step Green Method of Synthesis of Activated Carbon from Lignocellulosic Biomass Waste of Jacaranda mimosifolia for Sustainable Water Purification. Nature Environment & Pollution Technology, 24(3).

Pehlivan, E., & Cetin, S. (2009). Sorption of Cr (VI) ions on two Lewatit-anion exchange resins and their quantitative determination using UV–visible spectrophotometer. Journal of Hazardous Materials, 163(1), 448–453.

Peng, H., & Guo, J. (2020). Removal of chromium from wastewater by membrane filtration, chemical precipitation, ion exchange, adsorption electrocoagulation, electrochemical reduction, electrodialysis, electrodeionization, photocatalysis and nanotechnology: a review. Environmental chemistry letters, 18(6), 2055–2068.

Preisner, M. (2020). Surface Water Pollution by Untreated Municipal Wastewater Discharge Due to a Sewer Failure. Environmental Processes, 7(3), 767–780. https://doi.org/10.1007/s40710-020-00452-5

Qasem, N. A., Mohammed, R. H., & Lawal, D. U. (2021). Removal of heavy metal ions from wastewater: a comprehensive and critical review. Npj Clean Water, 4(1), 36.

Qu, J., Li, K., Wang, Q., Tong, W., Zhang, G., Hu, Q., Tao, Y., Jiang, Z., & Zhang, Y. (2024). Enhanced degradation of organic contaminant with bamboo shoot skin-based Fe/N co-doped porous hydrochar via persulfate activation. Journal of Cleaner Production, 441, 140881.

Rafi, D. M. (2018). Removal of heavy metal ions from wastewater by chemically modified agricultural waste material as potential adsorbent-a review. International Journal of Current Engineering and Technology.

Rahman, Z., & Singh, V. P. (2019). The relative impact of toxic heavy metals (THMs)(arsenic (As), cadmium (Cd), chromium (Cr)(VI), mercury (Hg), and lead (Pb)) on the total environment: an overview. Environmental Monitoring and Assessment, 191(7), 419.

Raji, Z., Karim, A., Karam, A., & Khalloufi, S. (2023). Adsorption of heavy metals: mechanisms, kinetics, and applications of various adsorbents in wastewater remediation—a review. Waste,

Rajoria, S., Vashishtha, M., & Sangal, V. K. (2022). Treatment of electroplating industry wastewater: a review on the various techniques. Environmental Science and Pollution Research, 29(48), 72196–72246.

Ran, S., Sun, K., Zhao, M., Wang, Z., Alshammari, A. S., Helal, M. H., El-Bahy, Z. M., Yuan, Y., & Fan, R. (2025). Metal-organic framework derived carbon-based composites for high-performance microwave absorption. Advanced Composites and Hybrid Materials, 8(1), 70.

Rasin, P., V, A. A., Basheer, S. M., Haribabu, J., Santibanez, J. F., Garrote, C. A., Arulraj, A., & Mangalaraja, R. V. (2025). Exposure to cadmium and its impacts on human health: A short review. Journal of Hazardous Materials Advances, 17, 100608. https://doi.org/https://doi.org/10.1016/j.hazadv.2025.100608

Rastin, H., Dell'Angelo, D., Sayede, A., Badawi, M., & Habibzadeh, S. (2025). Green and sustainable metal-organic frameworks (MOFs) in wastewater treatment: A review. Environmental Research, 282, 122087.

Ravina, Srivastava, G., Dalela, S., Kumar, S., Nasit, M., Singh, J., Ahmad, M. A., & Alvi, P. (2024). Study of structural, optical, surface and electrochemical properties of Co3O4 nanoparticles for energy storage applications. Interactions, 245(1), 85.

Ren, J., Huang, Y., Zhu, H., Zhang, B., Zhu, H., Shen, S., Tan, G., Wu, F., He, H., & Lan, S. (2020). Recent progress on MOF-derived carbon materials for energy storage. Carbon Energy, 2(2), 176–202.

Ronsse, F., Nachenius, R. W., & Prins, W. (2015). Carbonization of biomass. In Recent advances in thermo-chemical conversion of biomass (pp. 293–324). Elsevier.

Sadegh, H., Ali, G. A., Gupta, V. K., Makhlouf, A. S. H., Shahryari-Ghoshekandi, R., Nadagouda, M. N., Sillanpää, M., & Megiel, E. (2017). The role of nanomaterials as effective adsorbents and their applications in wastewater treatment. Journal of Nanostructure in Chemistry, 7(1), 1–14.

Saratale, R., Banu, R., Bharagava, R., & Saratale, G. (2018). Textile Industry Wastewaters as Major Sources of Environmental Contamination: Bioremediation Approaches for Its Degradation and Detoxification. In (pp. Chapter 8). https://doi.org/10.1007/978-981-13-1891-7_7

Satyam, S., & Patra, S. (2024). Innovations and challenges in adsorption-based wastewater remediation: A comprehensive review. Heliyon, 10(9).

Shao, D., Wang, C., Wang, L., Guo, X., Guo, J., Zhang, S., & Lu, Y. (2021). A N-doped Cobalt@ graphitized carbon material derived from ZIF-67 assisted polyvinylidene fluoride hollow fiber membrane for supercapacitors. Journal of Alloys and Compounds, 863, 158682.

Sharma, M., Kant, R., Sharma, A., & Sharma, A. (2025). Exploring the impact of heavy metals toxicity in the aquatic ecosystem. International Journal of Energy and Water Resources, 9(1), 267–280.

Sheoran, A., & Sheoran, V. (2006). Heavy metal removal mechanism of acid mine drainage in wetlands: a critical review. Minerals engineering, 19(2), 105–116.

Shree, B., Kumari, S., Singh, S., Rani, I., Dhanda, A., & Chauhan, R. (2025). Exploring various types of biomass as adsorbents for heavy metal remediation: A review. Environmental Monitoring and Assessment, 197(4), 406.

Singh, A., Sharma, A., Verma, R. K., Chopade, R. L., Pandit, P. P., Nagar, V., Aseri, V., Choudhary, S. K., Awasthi, G., & Awasthi, K. K. (2022). Heavy metal contamination of water and their toxic effect on living organisms. In The toxicity of environmental pollutants. IntechOpen.

Singh, S., Kapoor, D., Khasnabis, S., Singh, J., & Ramamurthy, P. C. (2021). Mechanism and kinetics of adsorption and removal of heavy metals from wastewater using nanomaterials. Environmental chemistry letters, 19(3), 2351–2381.

Sundararaman, S., Renita, A. A., Prabu, D., Kumar, J. A., Anish, M., Jayaprabakar, J., Prabu, R. T., Sathish, T., & Baigenzhenov, O. (2025). Elucidation of synthesis routes and adsorptive mechanisms in removal of water contaminants by MOF-derived carbon materials. Materials Science and Engineering: B, 315, 118093.

Tella, T. A., Festus, B., Olaoluwa, T. D., & Oladapo, A. S. (2025). Water and wastewater treatment in developed and developing countries: Present experience and future plans. In Smart nanomaterials for environmental applications (pp. 351–385). Elsevier.

Topare, N. S., & Wadgaonkar, V. S. (2023). A review on application of low-cost adsorbents for heavy metals removal from wastewater. Materials Today: Proceedings, 77, 8–18.

Uysal, M., & Ar, I. (2007). Removal of Cr (VI) from industrial wastewaters by adsorption: Part I: Determination of optimum conditions. Journal of Hazardous Materials, 149(2), 482–491.

Wang, J., & Chen, B. (2015). Adsorption and coadsorption of organic pollutants and a heavy metal by graphene oxide and reduced graphene materials. Chemical Engineering Journal, 281, 379–388.

Wang, L. K., & Wang, M.-H. S. (2025). Environmental management of electroplating and metal-finishing operations. In Control of heavy metals in the environment (pp. 325–378). CRC Press.

Wang, L. K., Wang, M.-H. S., Shammas, N. K., & Hahn, H. H. (2021). Physicochemical treatment consisting of chemical coagulation, precipitation, sedimentation, and flotation. In Integrated natural resources research (pp. 265–397). Springer.

Wang, X., Guo, Y., Yang, L., Han, M., Zhao, J., & Cheng, X. (2012). Nanomaterials as sorbents to remove heavy metal ions in wastewater treatment. J. Environ. Anal. Toxicol, 2(7), 154–158.

Wei, H., Rao, Y., Liu, J., Wang, Y., & Cao, Y. (2024). Impact on urban river water quality and pollution control of water environmental management projects based on SMS-Mike21 coupled simulation. Scientific Reports, 14(1), 6492. https://doi.org/10.1038/s41598-024-57201-z

Xiao, W., Cheng, M., Liu, Y., Wang, J., Zhang, G., Wei, Z., Li, L., Du, L., Wang, G., & Liu, H. (2023). Functional metal/carbon composites derived from metal–organic frameworks: insight into structures, properties, performances, and mechanisms. ACS Catalysis, 13(3), 1759–1790.

Yang, J., Hou, B., Wang, J., Tian, B., Bi, J., Wang, N., Li, X., & Huang, X. (2019). Nanomaterials for the removal of heavy metals from wastewater. Nanomaterials, 9(3), 424.

Yang, X., Wang, X., Xu, S., Lu, B., Huang, B., Zheng, X., & Lin, G. (2024). ZIF-67 and biomass-derived N, S-codoped activated carbon composite derivative for high-effective removal of hydroquinone from water. ACS applied materials & interfaces, 16(26), 34254–34265.

Yu, G., Lu, Y., Guo, J., Patel, M., Bafana, A., Wang, X., Qiu, B., Jeffryes, C., Wei, S., & Guo, Z. (2018). Carbon nanotubes, graphene, and their derivatives for heavy metal removal. Advanced Composites and Hybrid Materials, 1(1), 56–78.

Yu, X., Sui, Q., Lyu, S., Zhao, W., Liu, J., Cai, Z., Yu, G., & Barcelo, D. (2020). Municipal Solid Waste Landfills: An Underestimated Source of Pharmaceutical and Personal Care Products in the Water Environment. Environmental Science & Technology, 54(16), 9757–9768. https://doi.org/10.1021/acs.est.0c00565

Yusuf, M. O. (2023). Bond characterization in cementitious material binders using Fourier-transform infrared spectroscopy. Applied Sciences, 13(5), 3353.

Zapata, J. G., Vangipuram, B., Dalin, C., & Erfani, T. (2023). Water Quality and Pollution Trading: A Sustainable Solution for Future Food Production. ACS ES&T Engineering, 3(8), 1112–1124. https://doi.org/10.1021/acsestengg.2c00383

Zhang, Y., Sam, E. K., Liu, J., & Lv, X. (2023). Biomass-based/derived value-added porous absorbents for oil/water separation. Waste and Biomass Valorization, 14(10), 3147–3168.

Zhao, Y., & Duan, L. (2025). Beyond Pollution Control: Transforming Agricultural Effluents into Strategic Water–Energy–Nutrient Assets. ACS Agricultural Science & Technology, 5(8), 1569–1571. https://doi.org/10.1021/acsagscitech.5c00471

Zhou, K., Mousavi, B., Luo, Z., Phatanasri, S., Chaemchuen, S., & Verpoort, F. (2017). Characterization and properties of Zn/Co zeolitic imidazolate frameworks vs. ZIF-8 and ZIF-67. Journal of Materials Chemistry A, 5(3), 952–957.

Zou, J., He, L., Jin, W., Mei, F., Tang, X., Cai, G., Cheng, D., & Wang, X. (2024). In-situ immobilization of ZIF-67/ZIF-8 on wood biomass for degradation of methylene blue and formaldehyde. Industrial Crops and Products, 221, 119327. https://doi.org/https://doi.org/10.1016/j.indcrop.2024.119327

Appendices

Appendix I: Plant Herbarium and its Identification

Appendix II: Plant Identification Report

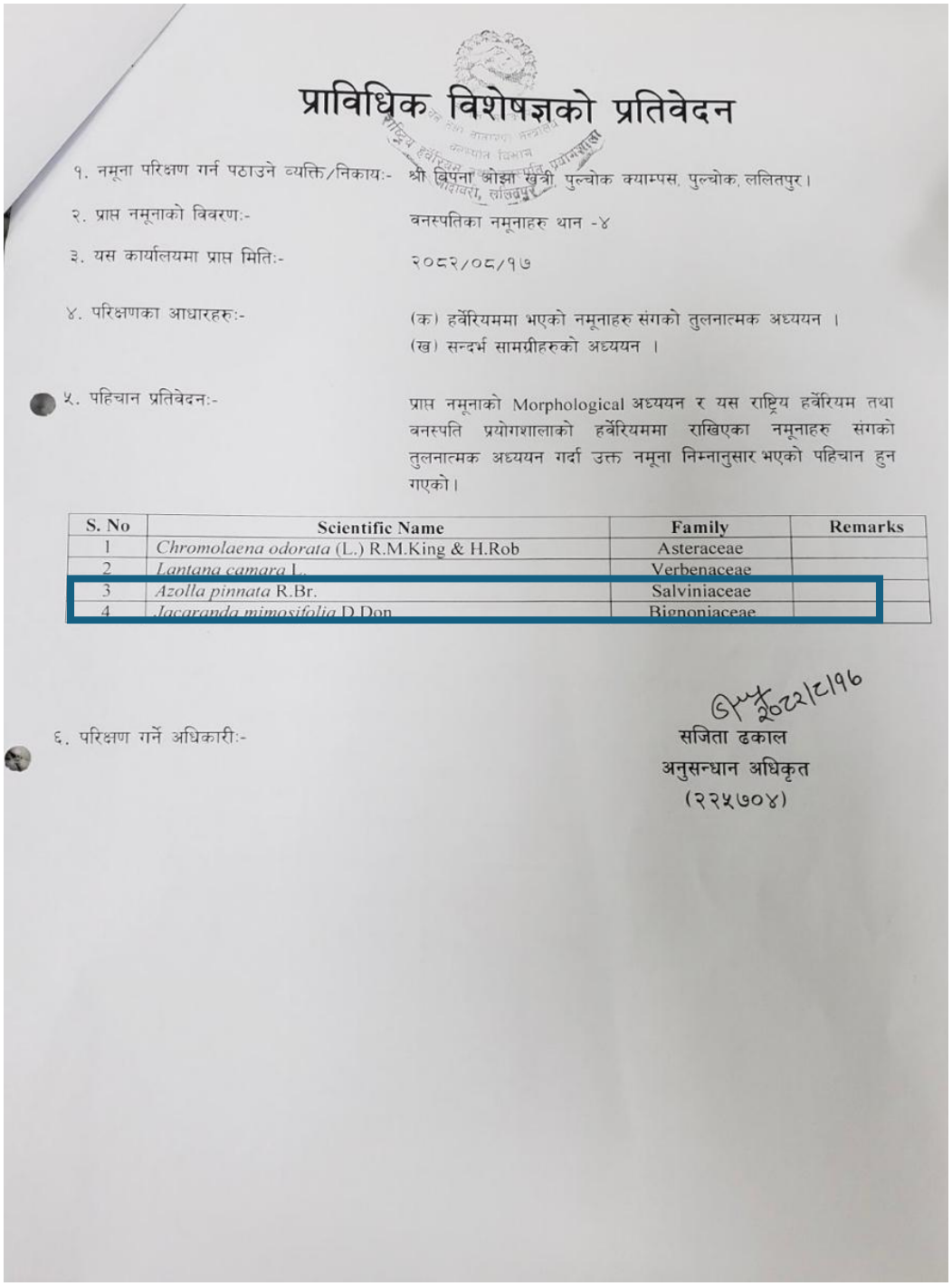

प्राविधिक विशेषज्ञको प्रतिवेदन

१. नमूना परिक्षण गर्न पठाउने व्यक्ति/निकायः- श्री बिपना ओझा खत्री पुल्चोक क्याम्पस, पुल्चोक, ललितपुर।

२. प्राप्त नमूनाको विवरणः- वनस्पतिका नमूनाहरु थान -४

३. यस कार्यालयमा प्राप्त मितिः- २०८२/०८/१७

४. परिक्षणका आधारहरुः- (क) हर्बेरियममा भएको नमूनाहरु संगको तुलनात्मक अध्ययन ।
(ख) सन्दर्भ सामग्रीहरुको अध्ययन ।

५. पहिचान प्रतिवेदनः- प्राप्त नमूनाको Morphological अध्ययन र यस राष्ट्रिय हर्बेरियम तथा वनस्पति प्रयोगशालाको हर्बेरियममा राखिएका नमूनाहरु संगको तुलनात्मक अध्ययन गर्दा उक्त नमूना निम्नानुसार भएको पहिचान हुन गएको।

S. No	Scientific Name	Family	Remarks
1	*Chromolaena odorata* (L.) R.M.King & H.Rob	Asteraceae	
2	*Lantana camara* L.	Verbenaceae	
3	*Azolla pinnata* R.Br.	Salviniaceae	
4	*Jacaranda mimosifolia* D.Don	Bignoniaceae	

६. परिक्षण गर्ने अधिकारीः-

२०२२/८/१६

सजिता ढकाल
अनुसन्धान अधिकृत
(२२५७०४)

Appendix III: Conference Certificate of IOE Graduate Conferences

IOE Graduate Conference

Certificate of Participation

This certificate is awarded to

Bibek Ghimire

in recognition of an invaluable contribution to
the academic discourse and research dessimination
at the 18th IOE Graduate Conference held from May 7 to 9, 2026
organized by Pulchowk Campus, Lalitpur, Nepal
through the Paper Presentation entitled

"Metal Organic Framework derived Carbon Composites from Jacaranda Seed Pods for Selective Removal of Cr(VI)."

Prof. Sangeeta Singh
Conference Convener

Prof. Sanjay Uprety
Champus Chief, Pulchowk Campus

Prof. Sushil Bahadur Bajracharya
Dean, Institute of Engineering

Appendix IV: Photographs during the work

<table>
<tr>
<td> 
Jacaranda Blooming at Pulchowk Campus Premises</td>
<td> 

Carbonization Tube Furnance</td>
</tr>
<tr>
<td> 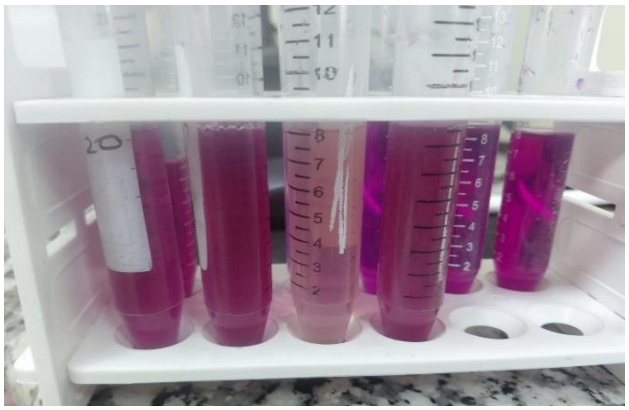
Adsorption of Cr(VI)</td>
<td> 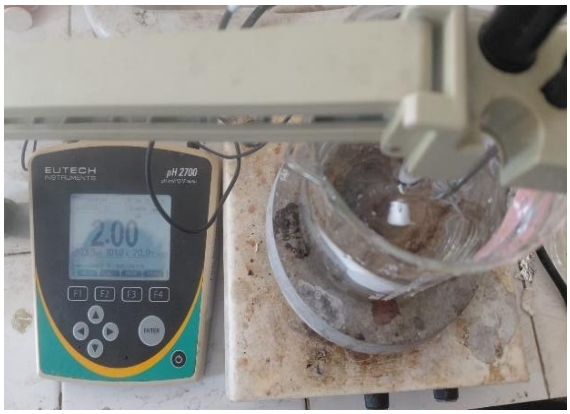

pH meter adjusting pH as 2.</td>
</tr>
</table>

Certificate After Presentation in IOEGC

Participation in IOEGC

Appendix V: Plagiarism Test

9% Overall Similarity

The combined total of all matches, including overlapping sources, for each database.

Filtered from the Report

- Bibliography
- Quoted Text
- Cited Text
- Small Matches (less than 8 words)

Match Groups

105 Not Cited or Quoted 9%
Matches with neither in-text citation nor quotation marks

0 Missing Quotations 0%
Matches that are still very similar to source material

0 Missing Citation 0%
Matches that have quotation marks, but no in-text citation

0 Cited and Quoted 0%
Matches with in-text citation present, but no quotation marks

Top Sources

9% Internet sources
6% Publications
0% Submitted works (Student Papers)

Integrity Flags

0 Integrity Flags for Review

No suspicious text manipulations found.

Our system's algorithms look deeply at a document for any inconsistencies that would set it apart from a normal submission. If we notice something strange, we flag it for you to review.

A Flag is not necessarily an indicator of a problem. However, we'd recommend you focus your attention there for further review.

Appreciation:

As this research project was funded by the Implementation of Urban Ecosystem-based Adaptation Research Activities Program implemented by the Nepal Academy of Science and Technology (NAST)-Nepal Climate Change Knowledge Management Centre (NCCKMC) in collaboration with Kathmandu Valley Development Authority (KVDA). The program is a part of the Urban Ecosystem-based Adaptation for Climate-resilient Development in the Kathmandu Valley, Nepal (Kathmandu Urban EbA Project) approved by the Global Environment Facility (GEF) with Least Developed Countries Fund (LDCF) and being executed by the KVDA with the technical oversight of the United Nations Environment Programme (UNEP).

Supported By: